resuspended in an induction medium (IM), which is composed of DMEM/F-12 supplemented with 1% NCS, 1× Antibiotic-Antimycotic, 1× Glutamax, 10 ng/mL BDNF and the inducing agent taurine (50 μmol/L) plus RA (10 μmol/L), then plated onto poly-D-lysine-coated 8-well culture slides to culture for an additional 8 days (Das *et al.* 2006; Osakada *et al.* 2008). Cells were fixed and immunocytochemistry was performed by staining the retinal photoreceptor markers rhodopsin and recoverin.

Real-time PCR

Real-time PCR was performed as previously described (Sugano *et al.* 2003). Total RNA was isolated from cultured cells using Trizol (Sigma). cDNA synthesis was carried out using the First-Strand cDNA Synthesis kit (GE Healthcare). SYBR Premix Ex Taq (Perfect Real Time; Takara) was used for PCR reactions. Specific transcripts were amplified on a Smart Cycler (Takara) for 35–40 cycles. The expression level of each gene was calculated by normalizing it with the glyceraldehyde 3-phosphate dehydrogenase (GAPDH) gene (TaqMan Rodent GAPDH Control Reagents; Applied Biosystems). The primers used in the experiment are shown in Table 1.

Immunocytochemical analysis

Immunocytochemistry was performed by staining cell-specific markers as previously described (Sugano *et al.* 2005; Das *et al.* 2006). Briefly, cells were fixed with 4% paraformaldehyde for 10 min at room temperature. After permeabilization with 0.3% Triton X-100 in phosphate-buffered saline (PBS) for 10 min, slides were incubated in 1% bovine serum albumin (BSA) and 5% blocking serum for 30 min at room temperature. Primary antibodies were added and incubated overnight at 4°C. The list of antibodies and their dilution are given in Table 2. Slides were washed and incubated with the secondary antibodies conjugated to Alexa Fluor 594 (red) or Alexa Fluor 488 (green) (Invitrogen-Molecular Probes) in the dark for 30 min at room temperature. A negative control was performed by replacing the primary antibody with normal IgG. For staining of nuclei, cells were covered with Vectashield medium including 4′6′-diamidino-2-phenylindole dihydrochloride (DAPI) (Vector Laboratories Inc.). Fluorescence was excited and labeled cells were imaged with a fluorescence microscope (Axiovert40; Zeiss, Germany).

Protein extraction and western blotting

Western blotting analysis was performed as previously described (Takahashi & Yamanaka 2006). Briefly, the NIH/3T3 cells were lysed with RIPA buffer supplemented with cocktail (Roche), and cell lysates (50 μg) were separated by electrophoresis on Mini-PROTEAN TGX gel (BIO-RAD) and transferred to an immuno-blot PVDF membrane (BIO-RAD). Antibodies used were Sox2, Nestin (1:200, shown in Table 2), anti-rabbit and anti-mouse IgG (H&L) AP conjugate (1: 7500, Promega).

Statistical analysis

The data of real-time PCR analysis are expressed as mean ± SD. Significance between groups was analyzed by one-way analysis of variance (ANOVA) with GraphPad Prism 4.0 software (San Diego). Values of $P < 0.05$ were considered statistically significant.

Results

NIH/3T3 fibroblasts can form neurosphere-like cells in defined conditions

First, we carried out a neurosphere assay on floating NIH/3T3 cells cultured in two different proliferating media: NSCm and NC. When NIH/3T3 cells were cultured in suspension for 2–5 days, NIH/3T3 cells formed spheres (Fig. 1B,C), which displayed classic features of neurospheres, in both proliferating media. There was no apparent difference in morphology between NC- and NSCm-cultured spheres for the first 2–3 days of culture. All NSCm-cultured spheres had a regular and round shape with bright borders on the edge of spheres (Fig. 1B). However, after 4–5 days of culture, the diameter of NC-cultured spheres did not increase, and some of these spheres showed an irregular and unhealthy appearance with dark or indistinct borders (Fig. 1C), which was assumed to be

Table 1. Sequences of primers used in real-time polymerase chain reaction (PCR)

Gene	Primer sequence (5′-3′) F	R	Product (bp)	Annealing temp. (°C)	GeneBank accession number
Nestin	AGACAGTGAGGCAGATGAGT	ATGAGAGGTCAGAGTCATGG	224	55	NM_016701
Sox2†	TAGAGCTAGACTCCGGGCGATGA	TTGCCTTAAACAAGACCACGAAA	296	60	NM_011443

†Primers of Sox2 were from Takahashi & Yamanaka (2006).

Table 2. List of antibodies used to stain different target cells

Antibody	Species	Dilution	Company and catalog no.	Target cells
Nestin	Mouse	1:500	Millipore-Chemicon:MAB353	Neural progenitors
Sox2	Rabbit	1:100	Santa Cruz Biotechnology, Inc: sc-20088	Neural progenitors
Msi1	Rabbit	1:100	Sigma-Aldrich: M3571	Neural progenitors
Pax6	Rabbit	1:100	Santa Cruz Biotechnology, Inc: sc-32766	Neural progenitors
BrdU	Mouse	1:100	Santa Cruz Biotechnology, Inc: sc-32323	Proliferating cells
β-tubulin	Mouse	1:500	Sigma: T5076	Neurons
NF200	Mouse	1:100	Sigma: N0142	Neurons
GFAP	Goat	1:100	Santa Cruz Biotechnology, Inc: sc-6171	Astrocytes
O4	Mouse	1:100	Chemicon International, Inc.: MAB345	Oligodendrocytes
Rhodopsin	Mouse	1:100	Millipore-Chemicon: MAB5316	Photoreceptors
Recoverin	Goat	1:100	Santa Cruz Biotechnology, Inc: sc-20353	Photoreceptors

BrdU, 5-Bromo-2′-deoxyuridine; GFAP, glial fibrillary acicic protein; Msi1, Musashi homologue 1; NF200, neurofilament 200 kDa; O4, oligodendrocyte marker O4; Pax6, paired box protein 6; Sox2, SRY (sex determining region Y)-box containing gene 2.

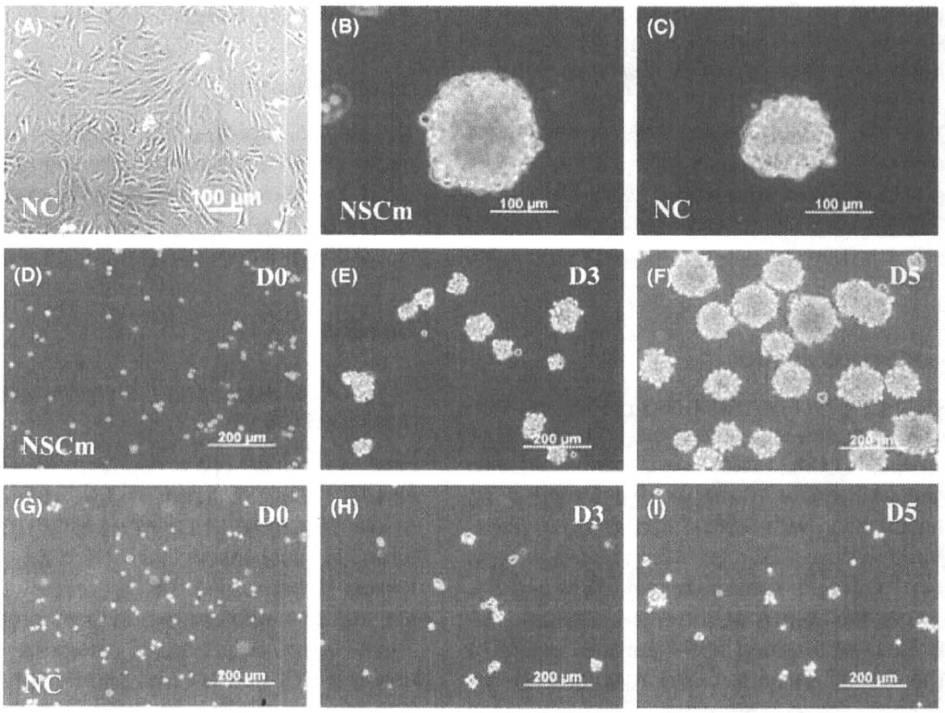

Fig. 1. Generation and passage of NIH/3T3-derived neurosphere-like cells. NIH/3T3 fibroblasts were adherently cultured in normal condition (NC) on normal (uncoated) dishes (A). Spheres were generated after culturing in neural stem cell medium (NSCm) (B) or NC (C) on 2% agarose-coated dishes for 5 days. Generation of the secondary spheres were carried out by culturing in NSCm (D–F) or NC (G–I) for 0, 3, and 5 days. The NSCm-cultured secondary spheres were observed on day 3 (E) after passaging, and the diameter had doubled by day 5 (F). NC-cultured spheres formed very small secondary spheres, and the diameter was unchanged after 3–5 days of culture (H and I).

surrounded by many dying cells caused by the lack of necessary growth factors.

Second, we tested the ability of NIH/3T3-derived spheres to generate secondary spheres. After dissociating into single cells and culturing for 3–7 days, the secondary spheres were quickly formed (on days 3–5) in NSCm, and the sphere size was dependent on culture time with defined cell density (Fig. 1D–F). These cells could generate sub-spheres for an extended period of three passages (more passages were untested). However, NC-cultured spheres formed only very small secondary spheres on days 3–5 after passaging (Fig. 1G–I), and tertiary spheres were difficult to generate.

NIH/3T3-derived spheres express neural progenitor markers

Third, we performed immunocytochemistry to stain the neural progenitor markers Nestin, Sox2, Pax6, and Msi1 for NSCm-cultured NIH/3T3-derived spheres, and the results showed that these cells expressed neural progenitor markers (Fig. 2E–T). Some of these spheres co-expressed Nestin and Sox2 (Fig. 2J–L), suggesting that some cells expressed multiple neural progenitor markers. Double staining for Sox2, Pax6, and Msi1 with BrdU indicated that these spheres were composed of dividing cells that entered the cell cycle (Fig. 2N–P,R,T).

To compare the neural progenitor potential of NIH/3T3 cells cultured in different conditions, the expression of neural progenitor markers Sox2 and Nestin were examined by real-time PCR. Sox2 (Fig. 2V) and Nestin (Fig. 2W) were significantly upregulated in NSCm-cultured spheres compared with adherent NIH/3T3 fibroblasts or NC-cultured spheres. Moreover, the expression of Nestin and Sox2 were also observed from NSCm-cultured spheres by western blotting (Fig. 2X).

NIH/3T3-derived spheres have the potential to differentiate into neuronal cells

Subsequently, we tested whether NIH/3T3-derived spheres can be differentiating into neuronal cells. After transferring to the DM, these spheres were cultured for another 8 days. Immunocytochemical results showed that these cells expressed the neuronal markers β-tubulin (Fig. 3D) and NF200 (Fig. 3H) and the astrocytic marker GFAP (Fig. 3K), although expression of GFAP was very low. However, these cells did not express the oligodendrocyte marker O4 (data not shown).

NIH/3T3-derived spheres can be induced to express retinal photoreceptor markers

Finally, to determine the ability of NIH/3T3 cells to differentiate along neural lineage, we treated NIH/3T3-derived neuron-like cells with taurine and RA, both of which show effective promotion of neuron induction. After treatment with these chemicals, expression of the neuronal marker β-tubulin (Fig. 4E) was greatly enhanced, and expression of photoreceptor markers rhodopsin (Fig. 4I,K,M) and recoverin (Fig. 4L,M) was also induced. Double staining results showed that some cells co-expressed recoverin and rhodospin (Fig. 4K–M); however, the expression of recoverin was very low (Fig. 4L–N). Real-time PCR analysis showed that neural progenitor markers Sox2 and Nestin were significantly downregulated during the differentiation and induction of neuron- and photoreceptor-like cells (Fig. 4O,P).

Discussion

Many studies have shown that the undifferentiated cells, such as ES cells, ES-derived neural stem cells (NSCs), bone marrow stromal cells or iPS cells have the ability to be differentiated along the neuronal lineage (Sanchez-Ramos *et al.* 2000; Woodbury *et al.* 2000; Zhao *et al.* 2002; Ikeda *et al.* 2005; Takahashi & Yamanaka 2006; Osakada *et al.* 2008, 2009; Hirami *et al.* 2009; Jin *et al.* 2009) and could be potential targets for the replacement therapy for retinal degeneration diseases. However, the ability of differentiated cells to be transdifferentiated into neuronal cells has not been widely investigated. Zhang *et al.* (2010) showed that the NIH/3T3 fibroblasts were able to be induced to express neuronal markers after the epigenetic modification by adding epigenetic modifiers, but the question of whether the differentiated cells could be transdifferentiated into neuronal cells without adding any epigenetic modifier and the mechanism involved still remain to be characterized.

Our study showed that NIH/3T3 fibroblasts were able to form spheres composed of dividing cells in suspension culture in the presence of EGF, bFGF and B27 supplement (without vitamin A), which are conditions suitable for the proliferation of neural progenitors. These spheres were able to be serially passaged to form more sub-spheres, and these cells were incorporated with BrdU, indicating their ability to self-renew. NSCm-cultured spheres express neural progenitor markers Nestin, Sox2, Pax6 and Msi1, indicating that these cells may have the potential to proliferate toward neural progenitor lineage. NIH/3T3-derived spheres was able to be differentiated into both neuronal and astrocytic cell types by removing EGF and B27 supplement (without vitamin A) from the medium and substituting them with serum, standard B-27 supplement and BDNF or CNTF, and also have the potential to be induced into photoreceptor-like cells. Taken together, these results suggested that NIH/3T3-derived neurosphere-like cells can undergo self-renewal and differentiation into neuron-like cells without any epigenetic modification, which are properties of neural progenitors, suggesting the possible neuronal lineage of NIH/3T3 fibroblasts.

To test whether the NIH/3T3-derived spheres obtained were neurospheres or neural progenitors, three functional attributes that define neural progenitors (or neural stem cells) must be exhibited. The first

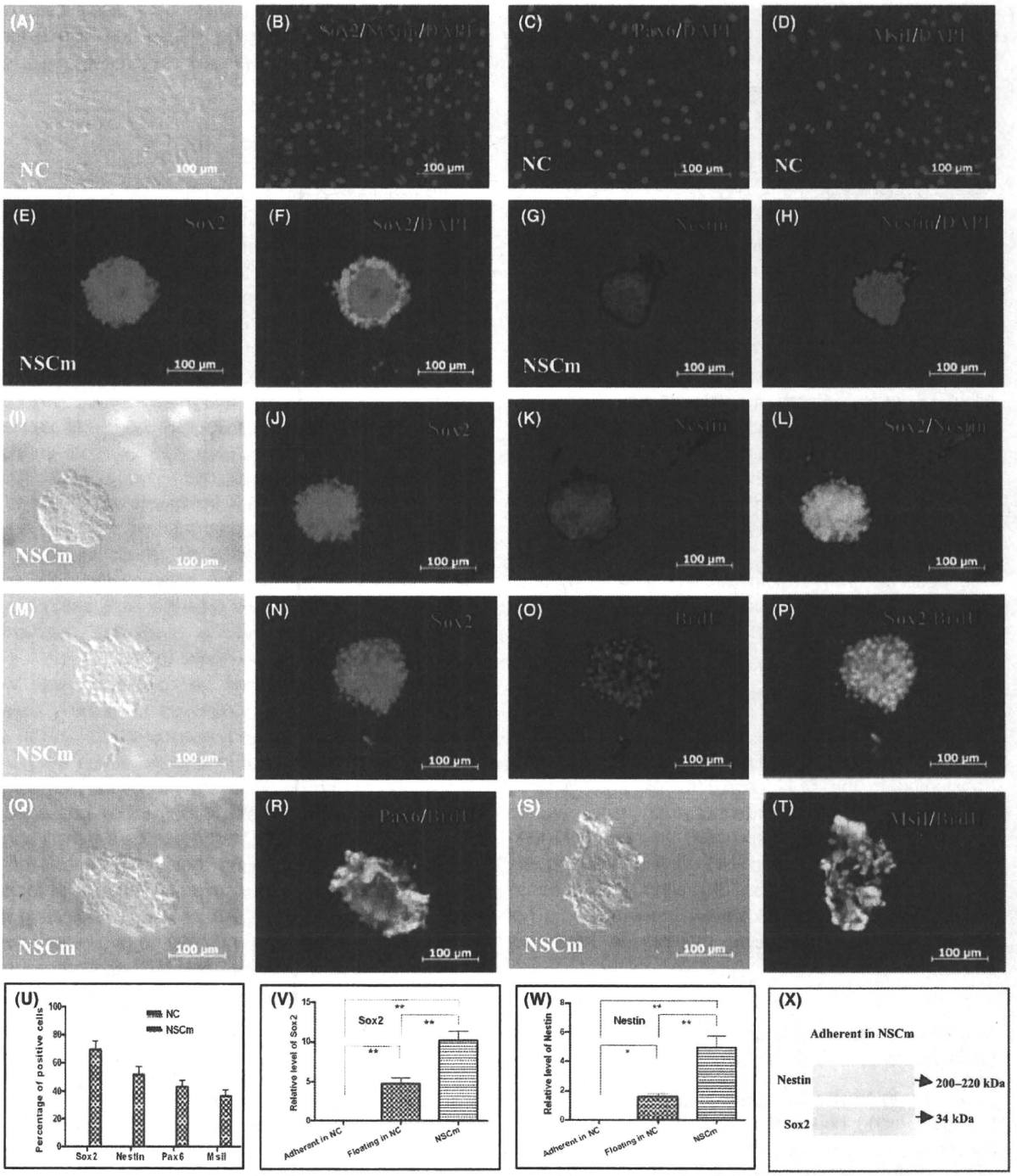

Fig. 2. Neural stem cell medium (NSCm)-cultured NIH/3T3-derived neurosphere-like cells expressed neural progenitor markers. NC-cultured NIH/3T3 fibroblasts did not express any neural progenitor marker (B–D). Single and double staining of Sox2 (E, F, J and L) and Nestin (G, H, K and L) demonstrated that these spheres co-expressed multiple neural progenitor markers. Some spheres were positively stained with BrdU and Sox2 (N-P), Pax-6 (R), Msi1 (T), indicating their proliferative property. Phase contrast images of NIH/3T3 cells cultured in NC (A) and NSCm (I, M, Q and S) were also shown. The percentage of positive cells is presented in the graph (U). Real-time PCR analysis of Sox2 (V) and Nestin (W) were performed for NIH/3T3 cells adherent in NC, floating in NC or NSCm. The columns represent the relative expression level of Sox2 or Nestin in spheres compared with those of adherent NIH/3T3 fibroblasts. Western blotting analysis of Sox2 and Nestin in NC- and NSCm-cultured NIH/3T3 cells were shown in X. The symbols * and ** represent $P < 0.05$ and $P < 0.01$, respectively.

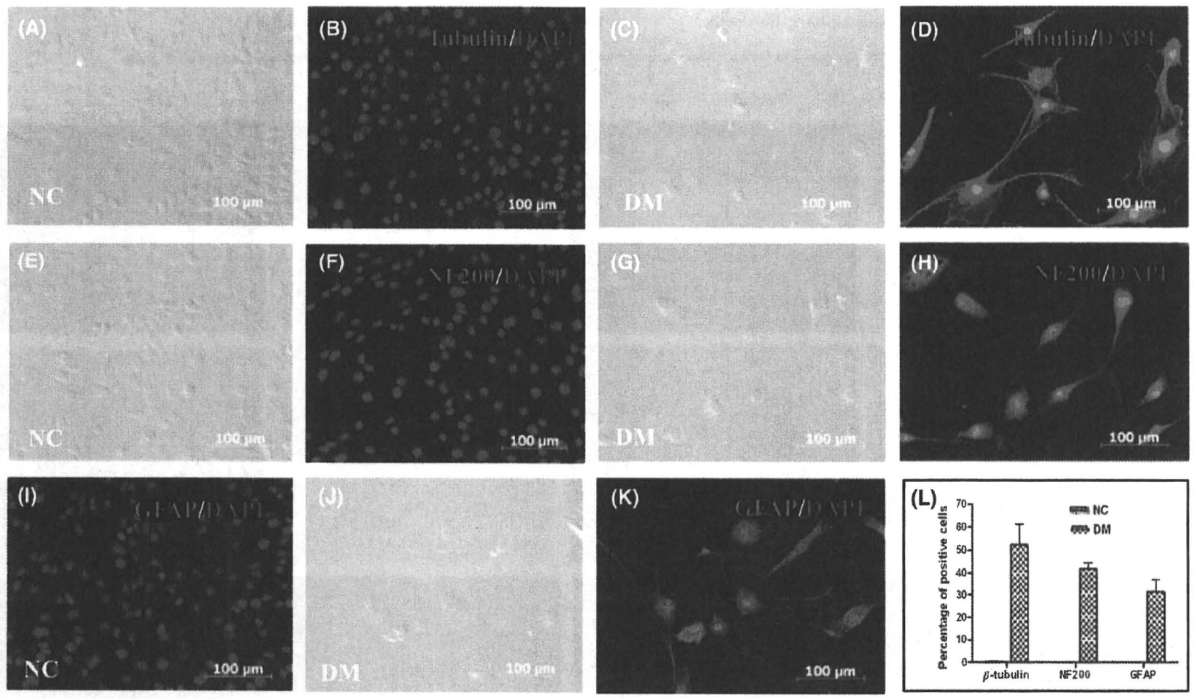

Fig. 3. Differentiation of neural stem cell medium (NSCm)-cultured NIH/3T3-derived neurosphere-like cells into neuron- and astrocyte-like cells. When shifted to DM, these cells expressed markers corresponding to neurons (β-tubulin [D] and NF200 [H]) and astrocytes (glial fibrillary acidic protein [GFAP] [K]). NIH/3T3 fibroblasts cultured in normal conditions (NC) were used as a control (A, B, E, F, and I). Phase contrast images of NIH/3T3 cells cultured in NC (A and E) and DM (C, G and J) were also shown. The percentage of positive cells expressing neuronal or glial markers is presented in the graph (L).

property is self-renewal wherein cells from spheres proliferate and make identical copies of themselves. The second is multipotency, wherein the spheres are able to generate all three main cell lineages of the mammalian central nervous system (CNS), neurons, astrocytes, and oligodendrocytes. The third is the ability to generate tissues. The generation of a neurosphere even from a particular region of the CNS does not necessarily denote to be neural progenitors unless there is supporting *in vivo* evidence (Chojnacki & Weiss 2008; Ahmed 2009). This neurosphere protocol has been used in a number of studies to examine the properties of various progenitors (Chaichana *et al.* 2006; Das *et al.* 2006; Jensen & Parmar 2006; Marshall *et al.* 2006; Chojnacki & Weiss 2008).

In the present study, we demonstrated the self-renewal property of NIH/3T3-derived spheres, and we also showed the potential of these cells to differentiate along two basic CNS lineages, neurons and astrocytes; however, we failed to show the expression of the oligodendrocyte marker O4.

These results predicted two possibilities. One is that these NIH/3T3-derived spheres are not neural progenitors, but only some NIH/3T3 cells with changes in morphology and properties. Because the growth of cells *in vivo* and *in vitro* are tightly regulated by their microenvironments (Hegde *et al.* 2007), NIH/3T3 fibroblasts are likely to survive in NSCm, display classic morphology of neurospheres and respond to growth factor exposure in a similar manner that was exhibited by neural progenitors. For example, the markers of neural progenitors were upregulated and some cells had the potential to differentiate toward neural lineage. However, most of these cells still preserved the property of NIH/3T3 fibroblasts, and could not be differentiated into all three main types of CNS lineages.

The other possibility is that these NIH/3T3-derived spheres may be immature neural progenitors. These spheres could proliferate, express markers of neural progenitors and generate neuron and astrocyte markers. The reason why these spheres did not express the oligodendrocyte marker O4 may be due to the lack of some growth factor(s) in the differentiating medium or the shortage of culture period, which may be critical for the generation of oligodendrocyte progenitors or oligodendrocytes. The cytokine CNTF alone might not be sufficient for the generation of oligodendrocytes, further investigations are needed to detect whether oligodendrocytes can be generated by adding other candidate factor(s), for example, platelet-derived

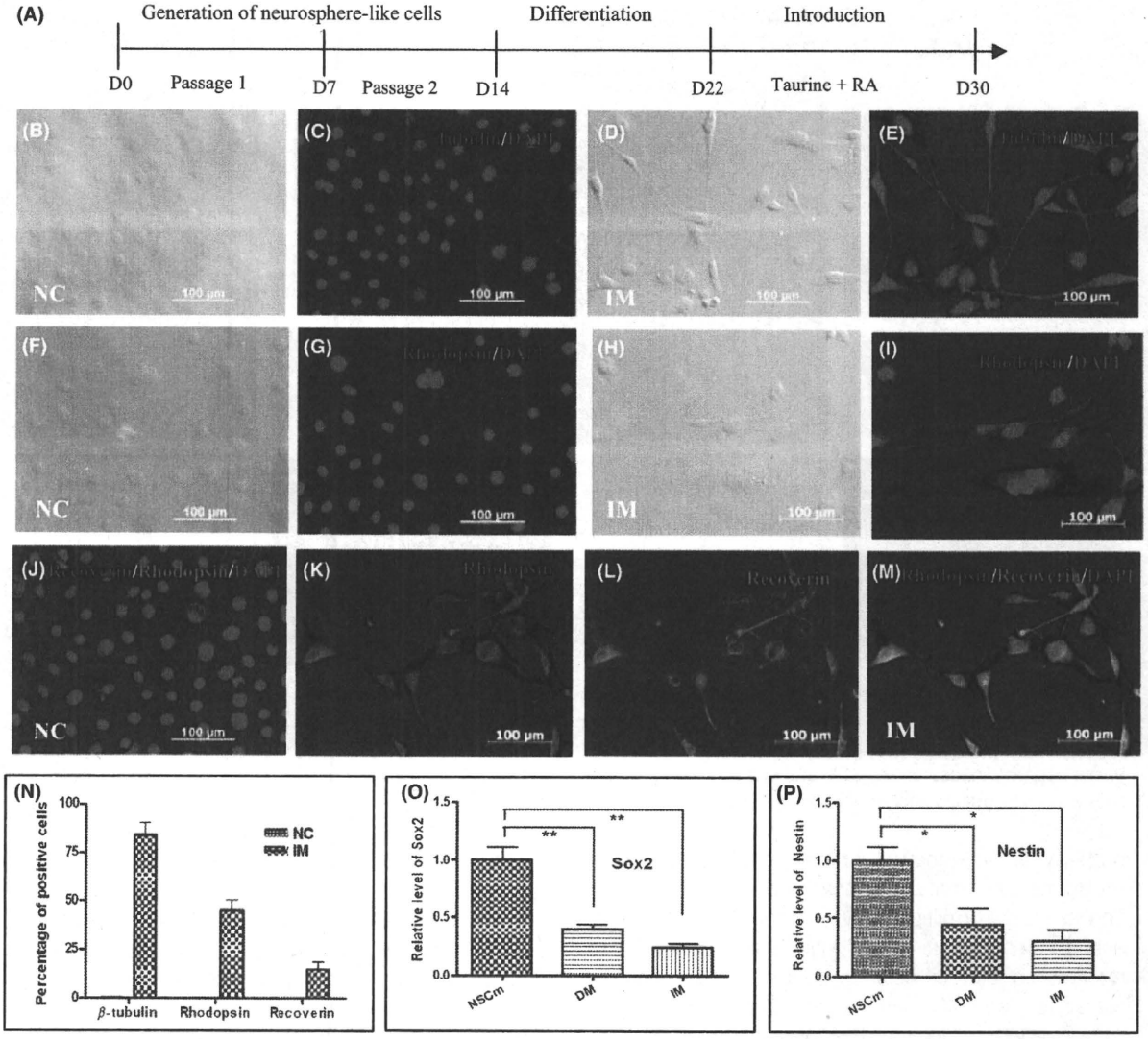

Fig. 4. Induction of neuron- and photoreceptor-like cells by treating cells with the combination of 50 μmol/L taurine and 10 μmol/L retinoic acid (RA). (A). Procedure for induction of retinal photoreceptor-like cells from NIH/3T3 fibroblasts. Immunocytochemical analysis of β-tubulin (C and E), rhodopsin (G, I, J, K and M) and recoverin (J, L and M) was performed for the treated (E, I, and K-M) and untreated (C, G and J) cells. Phase contrast images of NIH/3T3 cells cultured in NC (B and F) and IM (D and H) were also shown. The percentage of positive cells expressing neuronal or photoreceptor markers is presented in the graph (N). Real-time PCR was carried out to analyze Sox2 (O) and Nestin (P) expression in NSCm-, DM- and IM-cultured cells. The symbols * and ** represent $P < 0.05$ and $P < 0.01$, respectively.

growth factor AA, which was demonstrated to effectively enhance survival of oligodendrocyte progenitors (Yang *et al.* 2005; Chen *et al.* 2007).

Our study demonstrates that NIH/3T3 fibroblasts display some features of neural progenitors and express neuron, astrocyte and even photoreceptor markers under defined conditions. These results shed some light on the induction of retinal photoreceptors from a differentiated cell source. Further studies are necessary to determine if NIH/3T3 fibroblasts can be differentiated into functional neurons or photoreceptors, but the present study suggests that neuronal cells can be generated from differentiated cells of other types without the need of adding any epigenetic modifier.

Acknowledgments

This work was supported in part by the Ministry of Health, Labour and Welfare, Japan Foundation for Aging and Health and the Program for Promotion of Fundamental studies in Health Sciences of the National Institute of Biomedical Innovation (NIBIO).

References

Ahmed, S. 2009. The culture of neural stem cells. *J. Cell. Biochem.* **106**, 1–6.

Brewer, G. J. & Torricelli, J. R. 2007. Isolation and culture of adult neurons and neurospheres. *Nat. Protoc.* **2**, 1490–1498.

Chaichana, K., Zamora-Berridi, G., Camara-Quintana, J. & Quinones-Hinojosa, A. 2006. Neurosphere assays: growth factors and hormone differences in tumor and nontumor studies. *Stem cells* **24**, 2851–2857.

Chen, Y., Balasubramaniyan, V., Peng, J., Hurlock, E. C., Tallquist, M., Li, J. & Lu, Q. R. 2007. Isolation and culture of rat and mouse oligodendrocyte precursor cells. *Nat. Protoc.* **2**, 1044–1051.

Chojnacki, A. & Weiss, S. 2008. Production of neurons, astrocytes and oligodendrocytes from mammalian CNS stem cells. *Nat. Protoc.* **3**, 935–940.

Das, A. V., Mallya, K. B., Zhao, X., Ahmad, F., Bhattacharya, S., Thoreson, W. B., Hegde, G. V. & Ahmad, I. 2006. Neural stem cell properties of Müller glia in the mammalian retina: regulation by Notch and Wnt signaling. *Dev. Biol.* **299**, 283–302.

Hegde, G. V., James, J., Das, A. V., Zhao, X., Bhattacharya, S. & Ahmad, I. 2007. Characterization of early retinal progenitor microenvironment: presence of activities selective for the differentiation of retinal ganglion cells and maintenance of progenitors. *Exp. Eye Res.* **84**, 577–590.

Hirami, Y., Osakada, F., Takahashi, K., Okita, K., Yamanaka, S., Ikeda, H., Yoshimura, N. & Takahashi, M. 2009. Generation of retinal cells from mouse and human induced pluripotent stem cells. *Neurosci. Lett.* **458**, 126–131.

Hoffman, L. M. & Carpenter, M. K. 2005. Characterization and culture of human embryonic stem cells. *Nat. Biotechnol.* **23**, 699–708.

Holden, C. & Vogel, G. 2008. A seismic shift for stem cell research. *Science* **319**, 560–563.

Ikeda, H., Osakada, F., Watanabe, K., Mizuseki, K., Haraguchi, T., Miyoshi, H., Kamiya, D., Honda, Y., Sasai, N., Yoshimura, N., Takahashi, M. & Sasai, Y. 2005. Generation of Rx+/Pax6 + neural retinal precursors from embryonic stem cells. *Proc. Natl Acad. Sci. USA* **102**, 11331–11336.

Jensen, J. B. & Parmar, M. 2006. Strengths and limitations of the neurosphere culture system. *Mol. Neurobiol.* **34**, 153–161.

Jin, W., Xing, Y. Q. & Yang, A. H. 2009. Epidermal growth factor promotes the differentiation of stem cells derived from human umbilical cord blood into neuron-like cells via taurine induction in vitro. *In Vitro Cell. Dev. Biol. Anim.* **45**, 321–327.

Klassen, H. & Reubinoff, B. 2008. Stem cells in a new light. *Nat. Biotechnol.* **26**, 187–188.

Marshall, G. P., Reynolds, B. A. & Laywell, E. D. 2006. Using the neurosphere assay to quantify neural stem cells in vivo. *Curr. Pharm. Biotechnol.* **8**, 141–145.

Matsuda, N., Lu, H., Fukata, Y., Noritake, J., Gao, H. F., Mukherjee, S., Nemoto, T., Fukata, M. & Poo, M. M. 2009. Differential activity-dependent secretion of brain-derived neurotrophic factor from axon and dendrite. *J. Neurosci.* **29**, 14185–14194.

Osakada, F., Ikeda, H., Sasai, Y. & Takahashi, M. 2009. Stepwise differentiation of pluripotent stem cells into retinal cells. *Nat. Protoc.* **4**, 811–824.

Osakada, F., Ikeda, H., Mandai, M., Wataya, T., Watanabe, K., Yoshimura, N., Akaike, A., Sasai, Y. & Takahashi, M. 2008. Toward the generation of rod and cone photoreceptors from mouse, monkey and human embryonic stem cells. *Nat. Biotechnol.* **26**, 215–222.

Sanchez-Ramos, J., Song, S., Cardozo-Pelaez, F., Hazzi, C., Stedeford, T., Willing, A., Freeman, T. B., Saporta, S., Janssen, W., Patel, N., Cooper, D. R. & Sanberg, P. R. 2000. Adult bone marrow stromal cells differentiate into neural cells in vitro. *Exp. Neurol.* **164**, 247–256.

Sugano, E., Tomita, H., Abe, T., Yamashita, A. & Tamai, M. 2003. Comparative study of cathepsins D and S in rat IPE and RPE cells. *Exp. Eye Res.* **77**, 203–209.

Sugano, E., Tomita, H., Ishiguro, S., Abe, T. & Tamai, M. 2005. Establishment of effective methods for transducing genes into iris pigment epithelial cells by using adeno-associated virus type 2. *Invest. Ophthalmol. Vis. Sci.* **46**, 3341–3348.

Takahashi, K. & Yamanaka, S. 2006. Induction of pluripotent stem cells from mouse embryonic and adult fibroblast cultures by defined factors. *Cell* **126**, 663–676.

Woodbury, D., Schwarz, E. J., Prockop, D. J. & Black, I. B. 2000. Adult rat and human bone marrow stromal cells differentiate into neurons. *J. Neurosci. Res.* **61**, 364–370.

Yamanaka, S. 2007. Strategies and new developments in the generation of patient-specific pluripotent stem cells. *Cell Stem Cell* **1**, 39–49.

Yamanaka, S. 2009. A fresh look at iPS cells. *Cell* **137**, 13–17.

Yang, Z. S., Watanabe, M. & Nishiyama, A. 2005. Optimization of oligodendrocyte progenitor cell culture method for enhanced survival. *J. Neurosci. Methods* **149**, 50–56.

Zhang, X. M., Li, Q. M., Su, D. J., Wang, N., Shan, Z. Y., Jin, L. H. & Lei, L. 2010. RA induces the neural-like cells generated from epigenetic modified NIH/3T3 cells. *Mol. Biol. Rep.* **37**, 1197–1202.

Zhao, X., Liu, J. N. & Ahmad, I. 2002. Differentiation of embryonic stem cells into retinal neurons. *Biochem. Biophys. Res. Commun.* **297**, 177–184.

Zhou, H., Wu, S., Joo, J. Y., Zhu, S., Han, D. W., Lin, T., Trauger, S., Bien, G., Yao, S., Zhu, Y., Siuzdak, G., Schöler, H. R., Duan, L. & Ding, S. 2009. Generation of induced pluripotent stem cells using recombinant proteins. *Cell Stem Cell* **4**, 381–384.

Gene Therapy (2010), 1–9

www.nature.com/gt

ORIGINAL ARTICLE

Immune responses to adeno-associated virus type 2 encoding channelrhodopsin-2 in a genetically blind rat model for gene therapy

E Sugano[1], H Isago[1], Z Wang[1,2], N Murayama[1], M Tamai[3] and H Tomita[1,4,5]

We had previously reported that transduction of the channelrhodopsin-2 (ChR2) gene into retinal ganglion cells restores visual function in genetically blind, dystrophic Royal College of Surgeons (RCS) rats. In this study, we attempted to reveal the safety and influence of exogenous ChR2 gene expression. Adeno-associated virus (AAV) type 2 encoding ChR2 fused to Venus (rAAV-ChR2V) was administered by intra-vitreous injection to dystrophic RCS rats. However, rAAV-ChR2 gene expression was detected in non-target organs (intestine, lung and heart) in some cases. ChR2 function, monitored by recording visually evoked potentials, was stable across the observation period (64 weeks). No change in retinal histology and no inflammatory marker of leucocyte adhesion in the retinal vasculature were observed. Although antibodies to rAAV (0.01–12.21 $\mu g\,ml^{-1}$) and ChR2 (0–4.77 $\mu g\,ml^{-1}$) were detected, their levels were too low for rejection. T-lymphocyte analysis revealed recognition by T cells and a transient inflammation-like immune reaction only until 1 month after the rAAV-ChR2V injection. In conclusion, ChR2, which originates from *Chlamydomonas reinhardtii*, can be expressed without immunologically harmful reactions *in vivo*. These findings will help studies of ChR2 gene transfer to restore vision in progressed retinitis pigmentosa.
Gene Therapy advance online publication, 28 October 2010; doi:10.1038/gt.2010.140

Keywords: retinitis pigmentosa; channelrhodopsin-2; immunoreactivity; adeno-associated virus; retinal ganglion cells

INTRODUCTION

Retinitis pigmentosa (RP) is a group of diseases in which a gene mutation results in the death of photoreceptor cells. At present, approximately 40 genes have been identified as the causative agents (http://www.sph.uth.tmc.edu/retnet/; provided in the public domain by the University of Texas Houston Health Science Center, Houston, TX, USA). The initial visual impairment in patients with RP is night blindness, and patients lose their vision in the final stage of this disease following visual field loss.[1] Many trials have been conducted to identify agents that can protect photoreceptors and delay vision loss, but effective treatments have not been developed against progressed RP.

Although photoreceptor cells are often degenerated in the case of progressed RP, other inner neurons, including retinal ganglion cells (RGCs) are preserved.[2] It would be ideal to utilise the remaining retinal neurons to restore vision. We have been studying light-gated cation-selective membrane channel protein channelrhodopsin-2 (ChR2)[3] to induce photoreceptor function in retinal neurons such as RGCs[4,5] and ON bipolar cells.[6] We have already demonstrated that the responses induced by various stimulus frequencies (Hz) in ChR2-transduced rats are in no way inferior to those in normal rats,[7] as supported by the finding that ChR2-induced photocurrents are extremely fast.[8,9] Visual function was also well analysed by using transgenic rats with ChR2 transduction into RGCs: the spatial frequencies based on behavioural responses of photoreceptor-degenerated ChR2 transgenic rats were the same as those of normal rats.[10] These studies indicate that transfer of the ChR2 gene into the remaining retinal neurons is a useful method for restoring vision in progressed RP.

However, for clinical application of ChR2 therapy, some problems must be considered. First, this approach is a gene therapy. An immune response (mostly a problem with adenovirus- and herpes simplex virus-derived vectors)[11] may be caused by adeno-associated virus (AAV) and its incorporation into the host genome may lead to de-repression of tumour suppression genes.[12–14] Second, ChR2 is a protein originating from *Chlamydomonas reinhardtii*. It is important to study the systemic responses on virus vector application and long-term expression of the transgene product in humans. In this study, to reveal the safety and influence of exogenous ChR2 gene expression, we investigated the functional stability of the ChR2 gene and the possibility of harmful immune reactions caused by this gene therapy in a Royal College of Surgeons (RCS) rat model of RP.

RESULTS

Recording of visually evoked potentials (VEPs) in RCS rats

Although RGCs are maintained in aged RCS (*rdy/rdy*) rats, VEPs would be abolished because of the loss of light-evoked synchronous activities by photoreceptor cells. Indeed, VEPs were not evoked even

[1]Department of International Advanced Interdisciplinary Research, Institute for International Advanced Research and Education, Tohoku University, Sendai, Japan; [2]Japan Foundation for Aging and Health, Aichi, Japan; [3]School of Medicine, Tohoku University, Sendai, Japan; [4]United Centers for Advanced Research and Translational Medicine, School of Medicine, Tohoku University, Sendai, Japan and [5]Innovation of New Biomedical Engineering Center, Tohoku University, Sendai, Japan
Correspondence: Dr H Tomita, Department of International Advanced Interdisciplinary Research, Institute for International Advanced Research and Education, Tohoku University, 4-1 Seiryo-machi, Aoba-ku, Sendai 980-8575, Japan.
E-mail: hiroshi-tomita@iiare.tohoku.ac.jp
Received 9 June 2010; revised 29 August 2010; accepted 7 September 2010

by the maximum flash of the light-emitting diode in any of the 6-month-old RCS (*ryd/rdy*) rats. After confirmation of the loss of photoreceptor-derived function, AAV encoding ChR2 fused to Venus (rAAV-ChR2V) was administered by intra-vitreous injection into the left eye. The right eye was not treated and served as the control. At 2 weeks after the injection, VEPs were recorded in the right visual cortex. The amplitude peaked at 8 weeks but remained stable until 64 weeks after the injection (Figure 1). There was no recording from the left side of the visual cortex (data not shown). We could not record for longer periods than 64 weeks because the lifespan of RCS rats is about 2 years.

Viral dissemination to the organs

To determine systemic dissemination of rAAV after the injection, total ribonucleic acids were isolated from each organ after 6 months of rAAV-ChR2V administration. No rAAV-derived Venus expression was detected by reverse transcription-polymerase chain reaction (RT-PCR) analysis from the brain, liver, spleen and kidney (Figure 2). As expected, we detected the appropriate Venus protein expression from the rAAV-transduced retinas. Venus expression was unexpectedly detected in other organs (heart, lung and intestine) in some cases.

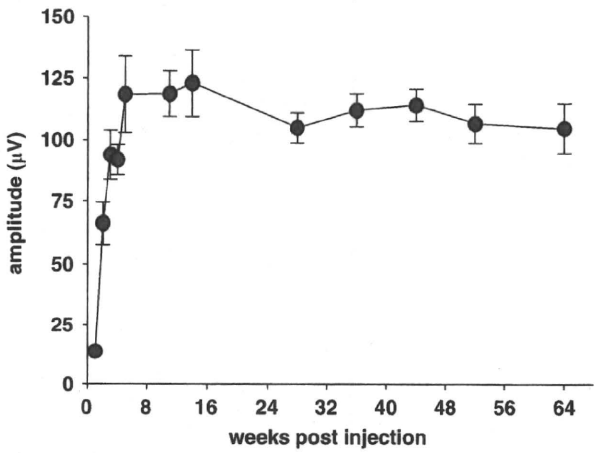

Figure 1 Long-term functional analysis of photosensitivity following ChR2 gene transfer by intra-vitreous injection of rAAV-ChR2V in 6-month-old RCS (*rdy/rdy*) rats. A blue LED (wavelength, 435–500 nm; peak, 470 nm) was flashed for 20 ms at 2.6 mW cm^{-2} and time-dependent improvements in the amplitude of the VEPs were recorded. After peaking at 8 weeks of administration, the amplitude remained stable for 64 weeks post-injection.

Histological examination of rAAV-ChR2V-treated retina

The rAAV-derived gene expression was investigated by observing whole-mounted retina. At 6 months after rAAV administration, the expression of ChR2V or Venus was observed by fluorescence microscopy (Figure 3). ChR2V was expressed in the plasma membrane of the retinal cells; on the other hand, Venus expression was observed in the cytoplasm of the rAAV-Venus-injected retina. Both of the rAAV-derived proteins were expressed all over the retina, and there was some deflection of the retinal expression.

To assess the side effects of ChR2 gene transfer by using rAAV, histological studies were performed on paraffin-embedded and frozen sections. There was no obvious difference in the retinal morphology between the ChR2-injected and the age-matched untreated RCS (*rdy/rdy*) rats (Figures 4a and b). However, intra-vitreous injection of lipopolysaccharide, which resulted in endotoxin-induced uveitis (EIU), in the RCS (+/+) rats caused substantial migration of inflammatory cells, mainly polymorphonuclear leucocytes, in the neural retina and vitreous humour (Figure 4d).

When the retinal activities were studied in frozen sections by immunohistochemistry (Figure 5), glial fibrillary acidic protein (GFAP) expression was restricted to the ganglion cell layers in the rAAV-ChR2V-treated retina (Figure 5c); however, GFAP expression was observed throughout the inner half of the retina in the untreated RCS (Figure 5b) and rAAV-Venus-injected RCS (Figure 5d) rats. Nuclear factor-κB (NF-κB) expression was restricted to the ganglion cell layers in all the tested RCS rats, but it was markedly high in the rAAV-ChR2V-treated retinas (Figure 5h).

Effects of rAAV-ChR2V treatment on leucocyte adhesion in the retinal vasculature

The retinal adherent leucocytes were imaged by perfusion labelling with fluorescein isothiocyanate-coupled concanavalin A. According to a report of Koizumi *et al.*,[15] leucocyte adhesion is significantly elevated

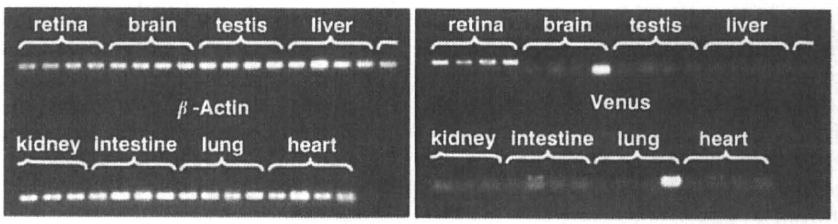

The expression of venus protein, which was carried by rAAV

	retina	brain	testis	liver	kidney	intestine	lung	heart
Sample1	+++	-	-	-	-	-	-	-
Sample2	+++	-	-	-	-	++	-	+
Sample3	+++	-	-	-	-	-	-	+
Sample4	+++	-	-	-	-	-	+	+

Abbreviations : -, No expression; +, Light expression; + +, Moderate expression; + + +, Intense expression;

Figure 2 Virus dissemination to the organs. At 6 months after the administration of rAAV-ChR2V, total ribonucleic acid was extracted from the retina, brain, testis, liver, kidney, intestine, lung and heart. The rAAV-derived gene was investigated by using RT-PCR analysis. As expected, a high copy number of the rAAV-derived gene expression was detected in the retina. The gene expression was also detected in the heart, lung and intestine in some cases.

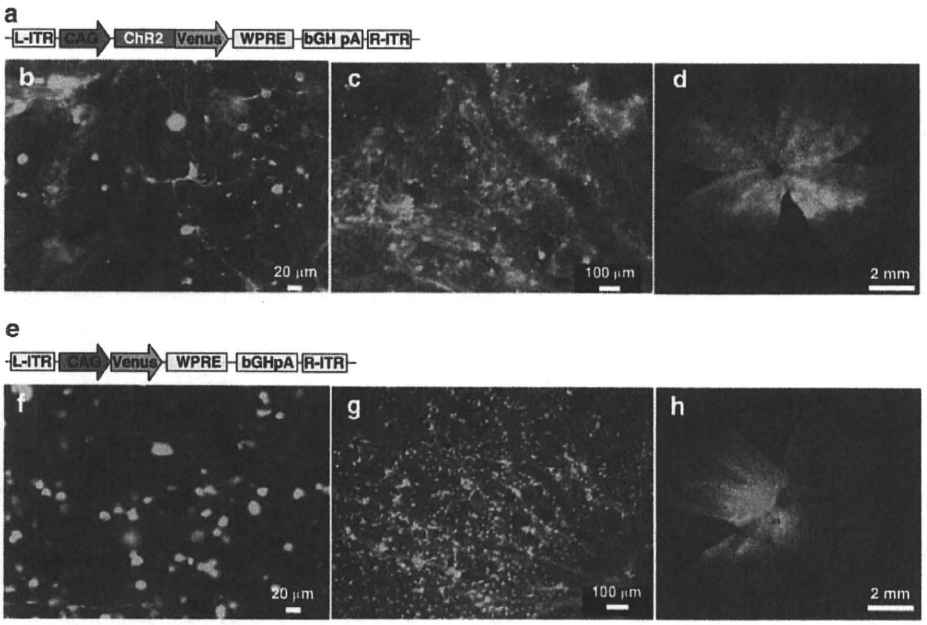

Figure 3 Expression profiles of the rAAV-derived proteins in the retina. Construction of the rAAV vector expressing ChR2V (**a**) and Venus (**e**) is illustrated. After 6 months of intra-vitreous injection, the rAAV-derived protein expression in whole-mounted retinal samples was observed by fluorescence microscopy. ChR2V expression was observed in the membrane (**b–d**) and Venus was expressed in the cytoplasm (**f–h**) of the retinal cells.

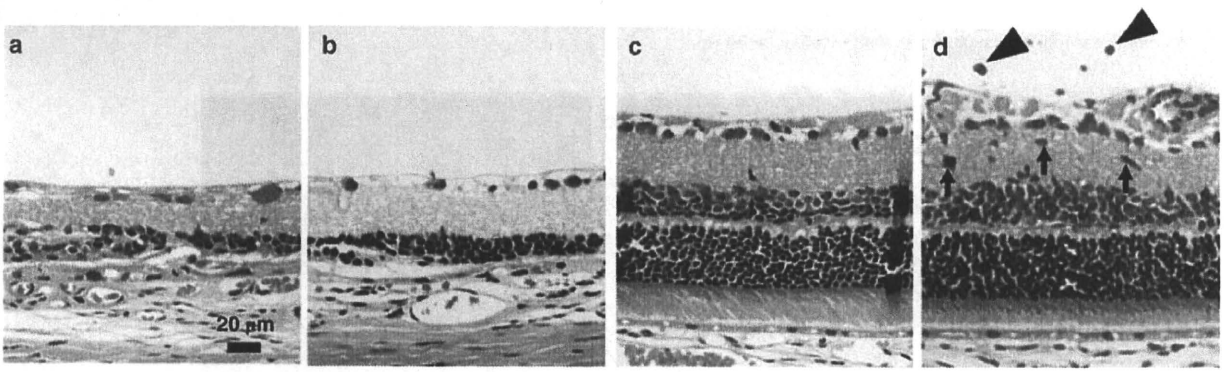

Figure 4 Histological examination of rAAV-ChR2V-treated retina. rAAV-ChR2V was administered by intra-vitreous injection into the left eye of RCS (*rdy/rdy*) rats. After 64 weeks, their right (control) (**a**) and left (**b**) eyeballs were enucleated and stained with hematoxylin and eosin. As a model of inflammation, age-matched RCS (+/+) rats were administered lipopolysaccharide (LPS) by intra-vitreous injection and their eyeballs were enucleated after 48 h. Retinal sections of untreated RCS (+/+) (**c**) and the LPS-treated (**d**) rats were studied. Substantial infiltration of inflammatory cells, which were mainly PMNLs in the neural retina (arrow) and vitreous humour (arrowhead), was observed in the retina of the LPS-treated rats.

after the development of EIU. Our study demonstrated that EIU caused leucocyte adhesion in the retinal venules (Figures 6c and d). However, there was no difference in leucocyte adhesion between the untreated (Figure 6a) and the rAAV-ChR2V-injected (Figure 6b) RCS rats, which had received the rAAV injection 1 year previously.

Humoral immune responses to the viral vector and transgene

To assess the possibility of a systemic humoral immune response to the viral vector or transgene, we determined the antibody levels against the rAAV2 capsid and ChR2 in serum by enzyme-linked immunosorbent assay. In the rAAV-ChR2V-injected rats, rAAV2 capsid-specific antibodies were detected and showed the maximum production at 2 months after injection (0.01–12.21 $\mu g\,ml^{-1}$; Figure 7a). However, the titre was extremely low in this study compared with that in a previous report of intramuscular injection of AAV2 (200–400 $\mu g\,ml^{-1}$).[16] The titre against the ChR2 protein was the maximum at 6 months post-injection. However, this level was also low (0–4.77 ± 2.55 $\mu g\,ml^{-1}$) compared with the antibody level in serum of the immunized rabbit (1442.34 $\mu g\,ml^{-1}$), which received a peptide injection to produce antibody to ChR2 forcibly (Figure 7b).

Analysis of T-lymphocyte subsets

Total T lymphocytes were gated with positive staining of anti-CD3. Then, the population of lymphocytes was confirmed by forward scatter (cell size) versus side scatter (cell granularity). Analysis of T lymphocyte subsets, namely $CD4^+$ (T helper cells), $CD8^+$ (cytotoxic

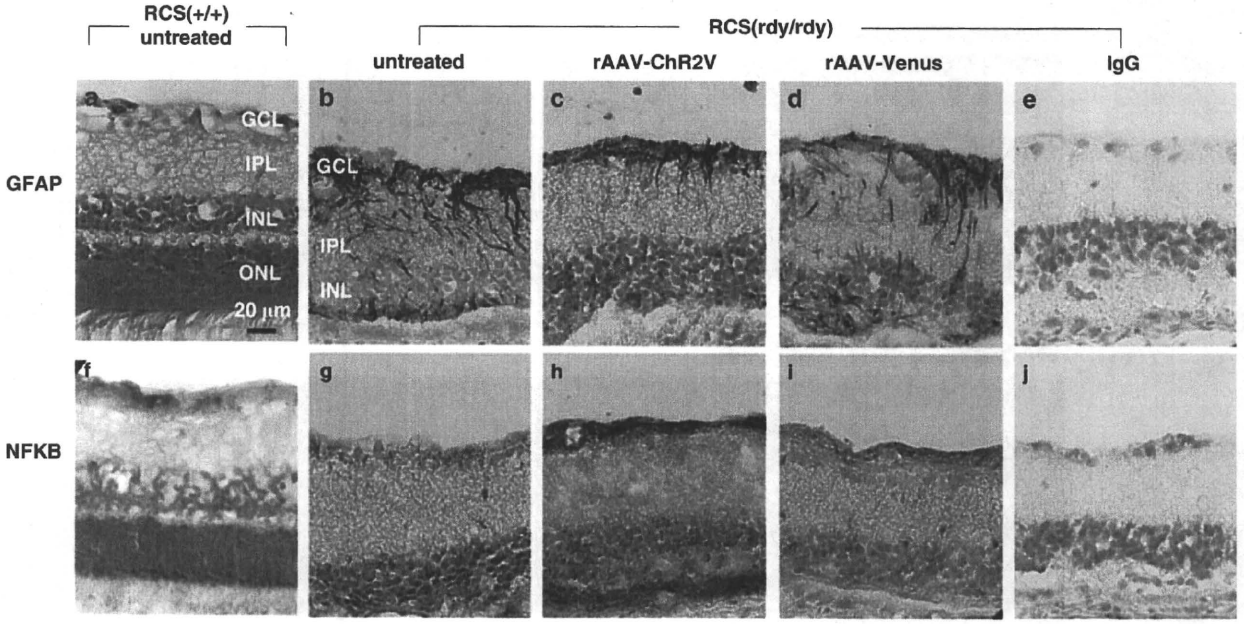

Figure 5 Changes in the protein immunoreactivities in the retina. Untreated RCS (+/+) (**a** and **f**) and RCS (*rdy/rdy*) (**b** and **g**) rats were used as the controls. rAAV-Venus (**d** and **i**) or rAAV-ChR2V (**c** and **h**) was administered by intra-vitreous injection into the left eye of RCS (*rdy/rdy*) rats. After 64 weeks, their eyeballs were enucleated. All the RCS rats were of the same age at the time of enucleation (2.2 years). As the negative control for staining, the first antibodies were replaced with non-immune mouse immunoglobulin G (**e** and **j**). DNA was counterstained with 4', 6-diamidino-2-phenylindole. GFAP expression was restricted to the ganglion cell and nerve fibre layers of the ChR2V-treated retina (**c**); however, it was observed throughout the inner half of the retina in the untreated RCS (**b**) and rAAV-Venus-injected RCS (**d**) rats. Nuclear factor-κB expression was restricted to the ganglion cell layers in all the tested RCS rats, but it was markedly high in the ChR2V-treated retina (**h**).

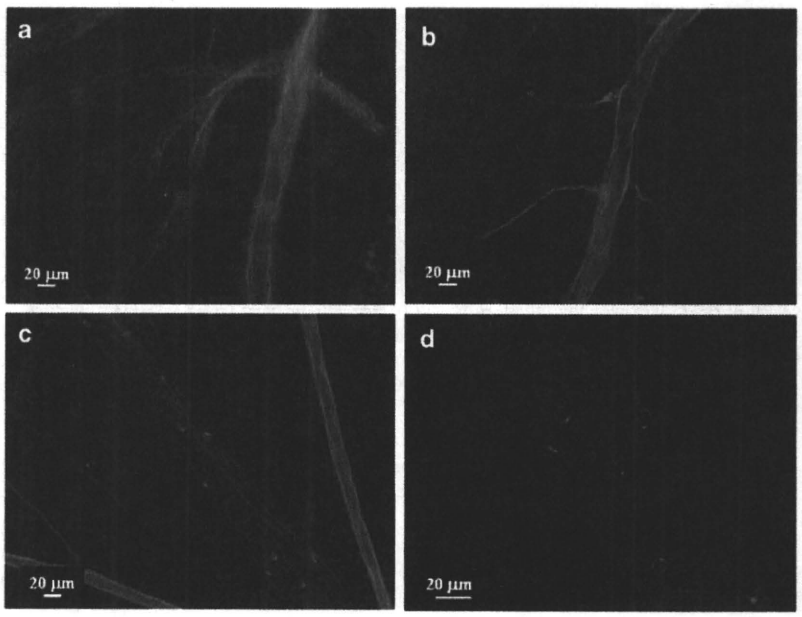

Figure 6 Adverse effect of rAAV-ChR2V treatment on retinal leucocyte adhesion. To study the adverse effect of ChR2 treatment in RCS rats, their retinas were examined after 1 year of rAAV-ChR2V injection. As a model of inflammation, RCS (+/+) rats received an intra-vitreous injection of lipopolysaccharide (LPS) and were examined 48 h after the injection. Flat-mounted retinas labelled with concanavalinA lectin showed increased number of adherent leucocytes in the retinal vessels of the LPS-injected rats (**c**) compared with the untreated (**a**) and rAAV-ChR2V-injected (**b**) rats. High-magnification photography of the LPS-treated retinal vessels showed leucocyte adhesion more clearly (**d**).

cells) and $CD4^+CD25^+$ (T regulatory cells), was performed. The $CD4^+/CD8^+$ ratio is a known indicator of the immunoregulatory status.[17,18] Our results demonstrated that the $CD4^+/CD8^+$ ratio after 1 week of the rAAV injection was higher than the pre-injection ratio (Figure 8a). This increase occurred in the case of both the rAAV-Venus and rAAV-ChR2V injections. In addition, the $CD4^+/CD8^+$ ratio only 1

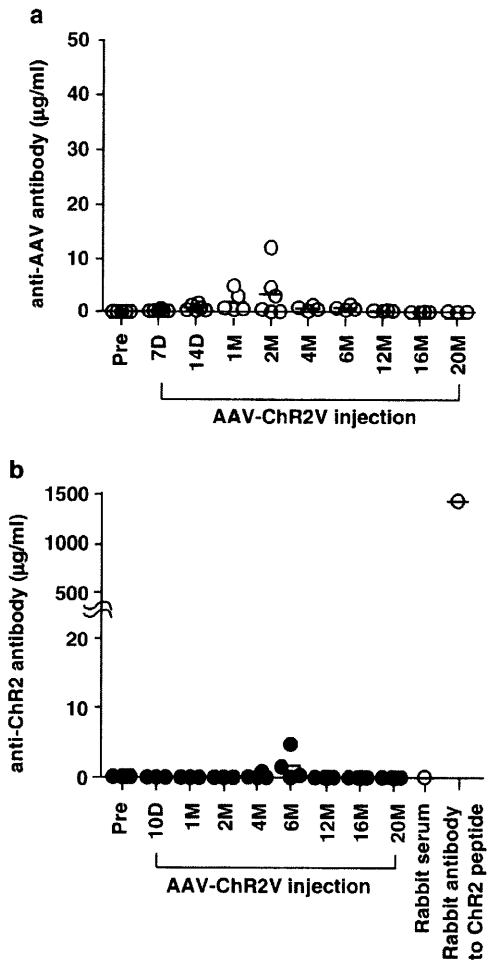

Figure 7 Humoral immune responses to the viral vector and transgene. Production levels of the antibodies to the AAV2 vector (**a**) and the therapeutic gene, ChR2 (**b**), were studied in RCS rats following a single intra-vitreous injection of rAAV-ChR2V. The time after injection is indicated. The antibody levels against both AAV2 and ChR2 were quite low compared with the antibody levels in serum of an immunized rabbit, which were considered as the effective dose to react with antigens.

month after the rAAV-ChR2V injection was higher than that before the injection. These data suggested that a change in the inflammation status occurred from 1 week to 1 month after rAAV administration. After this period, the ratios decreased to the pre-injection value and were stable for 1 year. To assess the inflammation status, we studied T regulatory cells. As shown in Figure 8b, a significant increase in the number of $CD4^+CD25^+$ cells was observed at 1 week after the rAAV-Venus and rAAV-ChR2V injections compared with the numbers before the injections. There was no significant difference in the inflammation status between the rAAV injections. As a positive control of inflammation, EIU also increased the population of $CD4^+CD25^+$ cells, which is consistent with a report by Toda *et al.*[19]

DISCUSSION

The results of this study demonstrate that the strategy of restoration of vision and light responses in photoreceptor-degenerated RCS (*rdy/rdy*) rats by rAAV-ChR2V administration was technically feasible and safe. Most importantly, ChR2 function, which was confirmed by measuring VEPs, was not reduced over the whole observation period after rAAV-ChR2V administration (Figure 1). A single administration of rAAV-ChR2V restored the light sensitivity over the lifespan of the rat model.

The eye is considered to be an immunologically protected space.[20] This immune privilege is the result of multiple layers and mechanisms, including the blood–retina barrier and other physical barriers, such as the immunosuppressive microenvironment against deviant systemic immunity, that limit the production of pro-inflammatory effector cells. We predicted that systemic dissemination of a virus would be limited by these immune systems after intra-vitreous injection. To investigate the systemic dissemination of rAAV, ribonucleic acids were isolated from each organ and the expressions of the Venus protein, which was fused to rAAV-ChR2, were studied (Figure 2). Venus expression was notable in the retina. Contrary to our expectations, the expression was also detected in the intestine, lung and heart in some cases. The RCS (*rdy/rdy*) animal model, which genetically causes loss of photoreceptors, is reported to have some breakdown of the blood–retina barrier or other mechanisms.[21–24] Therefore, the rAAV vector might have been disseminated to the other organs. Supporting this hypothesis, the efficiency of rAAV-derived gene transfer was higher in RCS rats than in normal rats (data not shown). This result suggests that some breakdown of the retinal barriers increased the permeability to rAAV.

The genomes transferred by rAAV tend to persist in cells mainly in an episomal, non-integrated form.[25] The transferred genomes in episomal form are diluted by cell division. However, when rAAV-carried genomes are inserted into chromosomes of cells with high proliferation ability, the genomes are preserved. There were some differences in gene delivery by rAAV among the samples obtained from the intestine, lung and heart. These differences might be the result of differences in the insertion forms of the rAAV genomes.

In gene therapy, tumour formation caused by the insertion of a transgene into the genome has been reported.[12–14] We did not observe tumour formation in any of the rats that received the rAAV injections (data not shown). For more information regarding tumour formation, further studies are needed by using methods such as Northern blotting, integration site analysis[26] and oncogene analysis.

We also investigated the inflammatory responses caused by the gene transfer by using the EIU model as a positive control of inflammation. EIU caused ocular inflammation, including leucocyte infiltration into the vitreous humour (Figure 4d) and leucocyte adhesion to the retinal vessels (Figures 6c and d). These findings are consistent with those of previous reports.[15,27] However, we did not observe such inflammatory cells in the retinas treated with rAAV-Venus or rAAV-ChR2V. Therefore, rAAV-ChR2V administration did not induce inflammation arising from bacterial infection.

GFAP is reportedly expressed because of gliosis and hypertrophy of macroglial cells.[28] Moreover, GFAP is expressed in astrocytes in the retina usually, but in Müller cells under pathological or stress conditions.[29] GFAP was also reported to be upregulated in the brain astrocytes during the inflammatory response.[30] Beurel and Jope[31] revealed that GFAP upregulation is caused by the production of the inflammatory cytokine interleukin-6. The absence of GFAP upregulation by viral injection (Figures 5b–d) demonstrates the lack of glial activation derived from inflammation. Our study showed that GFAP was expressed throughout the retina in the untreated RCS rats and that the expression was decreased and restricted by the rAAV-ChR2V injection (Figure 5c). These results reveal that activation of RGCs by ChR2 may have a protective effect on the inner retina.[32,33] NF-κB expression in the retina was restricted to the ganglion cell layers in all

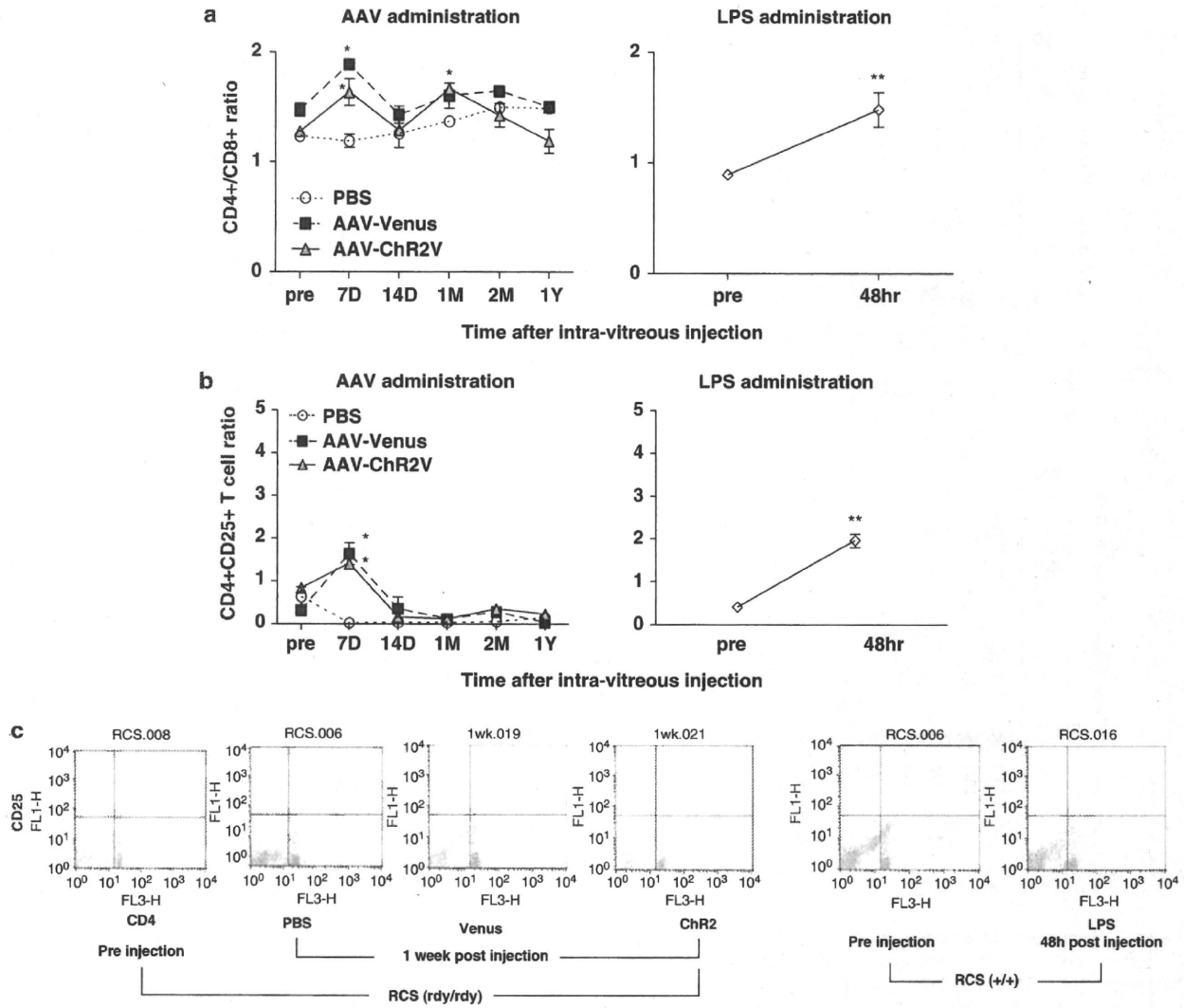

Figure 8 T-cell ratio in the peripheral blood. Lymphocytes were isolated from the peripheral blood before and after injection of PBS, rAAV-Venus or rAAV-ChR2V. The lymphocytes were incubated with anti-T-cell receptor-associated CD3, anti-CD4 and anti-CD8a mAbs, and analysed by flow cytometry. The blood of lipopolysaccharide-administrated rats as a positive control of inflammation was also analysed. The T-cell ratio of $CD4^+/CD8^+$ (**a**) and $CD4^+CD25^+$ (T regulatory cells) (**b**) was calculated. (**c**) Representative data of T regulatory analysis are indicated. All data are represented as the mean (s.d.) of four to seven animals.

the experiments and there was no staining of the other inner retinal cells, which was caused by stress.[34] We also demonstrated the potent expression of NF-κB p65 in the rAAV-ChR2V-injected retinas. These results are consistent with reports that constitutive NF-κB activity is the result of ongoing synaptic activity.[35,36]

The T-lymphocyte analysis demonstrated that the $CD4^+/CD8^+$ ratio was higher in all the rAAV-treated rats at 1 week after the injection than before the injection, and in the rAAV-ChR2V-treated rats, the ratio was high at 1 month after injection (Figure 8a). However, these increases were transient and returned to the pre-injection level. This expansion allows cross-talk between different types of cells in the ongoing immune response.[17] Kim and Lim[18] reported that $CD4^+/CD8^+$ expansion is caused by bacterial infection. After 1 week, the ratio increased in all the rAAV-injected rats. Thus, there might have been some immune reactions such as antigen presentation to rAAV. At 1 month after the rAAV-ChR2V injection, the ratio increased again. As shown in Figure 1, the maximum ChR2 function was recorded at 1 month in the visual cortex first. Thus, some immune reactions might have been induced by increased ChR2 expression but were well tolerated at 2 months after the injection.

Currently, the best characterized regulatory cells are $CD4^+CD25^+$ T cells.[37] These cells can suppress host immune responses and modulate the immune responses in autoimmune diseases, allergy, transplantation and infectious diseases.[38,39] CD25, an interleukin-2 receptor, is reported to be an inflammation marker on $CD4^+$ lymphocytes.[18] In the EIU experiment, we observed expansion of $CD4^+CD25^+$ cells, which is consistent with the report by Toda *et al.*[19] A significant increase in the number of $CD4^+CD25^+$ cells was observed in both the rAAV-Venus and the rAAV-ChR2V rats at 1 week after the injections compared with the pre-injection values (Figure 8b), although there was no significant difference in the results between the rAAV-Venus and the rAAV-ChR2V injections.

These results demonstrate that the inflammation-like immunological reaction was caused by AAV and not by ChR2.

To assess the possibility of a systemic humoral immune response to the viral vector or transgene product, we measured the antibody levels of the rAAV2 capsid and ChR2 in serum by enzyme-linked immunosorbent assay. Intra-vitreous injection caused relatively little antibody production (Figure 7a) compared with the different route of AAV injection used by Zhang *et al.*[16] Li *et al.*[40] demonstrated that a single intra-vitreous injection of AAV2 causes increased AAV antibody production at 2 months after injection. Our data are consistent with their report in terms of the timing of increase and the amount of antibody production (Figure 7a). We anticipated that ChR2 expression would cause antibody production because ChR2 is not inherent to humans. However, the production levels were relatively low (Figure 7b) and were insufficient to induce a humoral immune response.

In conclusion, an immune reaction can be caused by AAV administration and ChR2 protein expression, but will be well tolerated. It should be noted that the experiments were performed in rats and cannot be directly extrapolated to humans, who constitute a far more immunologically heterogeneous population. However, these findings will help studies of ChR2 gene transfer to restore vision in progressed RP.

MATERIALS AND METHODS

Animals

In total, 59 (6-month-old male) RCS rats (43 dystrophic (*rdy/rdy*)); 16 non-dystrophic (+/+) were used in this study (Table 1). The animals were maintained and used in accordance with the ARVO Statement for the *Use of Animals in Ophthalmic and Vision Research and the Guidelines for Animal Experiments of Tohoku University.* All the animal experiments were conducted with the approval of the Animal Research Committee, School of Medicine, Tohoku University. To compare the functions, the control and treated rats were age-matched in each experiment.

Induction of EIU

As a model of ocular inflammation,[41] RCS (+/+) rats received a single intra-vitreous injection of 5 μg lipopolysaccharide from *Escherichia coli* (055:B5; Sigma, St Louis, MO, USA) in 5 μl phosphate-buffered saline (PBS) to cause EIU. After 48 h of lipopolysaccharide administration, the inflammation status was studied.

Preparation of AAV vector carrying the ChR2 gene construct

The *N*-terminal fragment (residues 1–315) of ChR2 (GenBank accession no. AF461397) was fused to a fluorescent protein, Venus, in frame at the end of the ChR2-coding fragment described previously.[5] The ChR2V or Venus gene was introduced into the *Eco*RI and *Hin*dIII sites of the 6P1 plasmid.[42] The synapsin promoter was exchanged for a hybrid cytomegalovirus enhancer/chicken β-actin promoter,[42] and AAV-ChR2V and AAV-Venus were constructed. The pAAV-RC and p-Helper plasmids were obtained from Stratagene (La Jolla, CA, USA). Semi-confluent 293T cells on 15-cm plates were co-transfected with split-packaging plasmids—AAV-ChR2V (or AAV-Venus), pAAV-RC and p-Helper—by using a calcium phosphate-based protocol according to the manufacturer's instructions (Agilent Technologies, La Jolla, CA, USA). The rAAV vectors (rAAV-ChR2V, rAAV-Venus) were purified by using the method of Auricchio *et al.*[43–45]

rAAV vector injection

The rAAV-ChR2V or rAAV-Venus vector was administered by intra-vitreous injection into the left eye of 6-month-old RCS (*rdy/rdy*) rats. In brief, the rats were anaesthetised by intramuscular injection of a mixture of ketamine (66 mg ml^{-1}) and xylazine (33 mg kg^{-1}). Under an operating microscope, the conjunctiva was incised to expose the sclera. A total volume of 5 μl of vector suspension at a concentration of 5×10^{12} genomic particles per μl was administered by intra-vitreous injection through the ora serrata with a 10-μl Hamilton syringe and a 32-gauge needle (Hamilton Company, Reno, NV, USA).

Recording of VEPs

VEPs were recorded by using Neuropack MEB-9102 (Nihon Kohden, Tokyo, Japan). The method of recording was derived from a combination of protocols used by Papathanasiou *et al.*[46] and Iwamura *et al.*[47] In brief, at least 7 days before the experiments, recording electrodes (silver–silver chloride) were placed epidurally on each side 7 mm behind the bregma and 3 mm lateral to the midline, and a reference electrode was placed epidurally on the midline 12 mm behind the bregma. Under ketamine–xylazine anaesthesia, the pupils were dilated with 1% atropine and 2.5% phenylephrine hydrochloride. The ground electrode clip was placed on the tail. Photic stimuli of 20-ms duration were applied at a frequency of 0.5 Hz and generated by pulse activation of a blue light-emitting diode with light-emitting wavelengths in the range 435–500 nm (peak, 470 nm). A total of 100 consecutive response waveforms were averaged for the VEP measurements.

Table 1 The Number of samples examined in this study

	VEP	*PCR*	*Expression in retina (whole mount)*	*Histology (HE)*	*Immuno-histochemistry*	*Leukocyte adhesion*	*Antibody detection*	*Flow cytometry*	*Total (n)*
No treatment (+/+)				3	3	3			9
Pre-treatment (+/+)								7	7
LPS administration (+/+)				3		4		7	
No treatment (*rdy/rdy*)				3	3	3			9
Pre-injection for PBS (*rdy/rdy*)								4	4
After PBS injection (*rdy/rdy*)								4	
Pre-injection for rAAV-Venus (*rdy/rdy*)								4	10
After rAAV-Venus injection (*rdy/rdy*)			3		3			4	
Pre-injection for rAAV-ChR2V (*rdy/rdy*)	20						3–6	4	20
After rAAV-ChR2V injection (*rdy/rdy*)	20	4	3	3	3	3	3–6	4	

Abbreviations: ChR2V, channelrhodopsin-2 fused to Venus; HE, hematoxylin and eosin; LPS, lipopolysaccharide; PBS, phosphate-buffered saline; PCR, polymerase chain reaction; rAAV, adeno-associated virus type 2; VEP, visually evoked potential.

Ribonucleic acid isolation and rAAV-derived protein detection by RT-PCR analysis

Total ribonucleic acids were extracted (TRIreagent; Sigma) from the retina, brain, lung, testis, liver, kidney, intestine, lung and heart. cDNA was synthesised (First-Strand cDNA synthesis kit; GE Healthcare, Piscataway, NJ, USA) and the tracer fusion protein, Venus, expression was investigated by using a semi-quantitative RT-PCR method. As the individual internal control, we performed PCR with β-actin. The primer sequences were as follows: 5′-TCATGAAGTGT GACGTTGACATCCGT-3′ (sense) and 5′-CCTAGAAGCATTTGCGGTGCAC GATG-3′ (antisense) for β-actin; 5′-GACGTAAACGGCCACAAGTT-3′ (sense) and 5′-GAACTCCAGCAGGACCATGT-3′ (antisense) for Venus. Following electrophoresis on 1.0% agarose gel, DNA was detected by staining with GelRed (Biotium, Inc., Hayward, CA, USA).

Histology

After death, the eyeballs were enucleated, immersed in 4% paraformaldehyde in PBS overnight at 4 °C and embedded in paraffin. Serial sections (4 μm) of whole eyes were cut sagittally, through the cornea and parallel to the optic nerve, and stained with haematoxylin and eosin. Microscopic examination of the sections was then performed (AxioImager A1; Carl Zeiss, Tokyo, Japan).

The ChR2V expression profile in the retina was studied according to the method we previously described.[5] In brief, the eyes were fixed and the retinas were flat-mounted on slides. Venus fluorescence was visualised under a fluorescence microscope (BZ-9000; Keyence Corp., Osaka, Japan).

Immunohistochemistry

Rat eyes were fixed overnight at 4 °C in 4% paraformaldehyde in PBS (pH 7.4). The retinas were rinsed with PBS and immersed in 10, 20 and 30% sucrose in PBS at 4 °C. Samples were embedded in optimal cutting temperature compound (Sakura, Tokyo, Japan) under liquid nitrogen and stored at −80 °C. Cryosections (10 μm) of tissue were mounted on slides and air dried. Then, retinal sections were washed with PBS and treated for 15 min with 0.3% H_2O_2 in methanol. After washing with PBS, the sections were incubated with mouse anti-rat NF-κB p65 (C-20) antibody (1:200; Santa Cruz Biotechnology, Santa Cruz, CA, USA) and mouse anti-rat GFAP antibody (1:250; Nihon Millipore, Tokyo, Japan) in antibody diluent buffer (0.05% Tween-20, 3% bovine serum albumin and 3% goat serum in PBS) overnight at 4 °C. After washing with 0.05% Tween-20 in PBS, the sections were incubated with horseradish peroxidase-conjugated goat anti-mus immunoglobulin G as the secondary antibody for 1 h at room temperature. After washing with TBST (150 mM NaCl, 0.1% Tween-20 in 20 mM Tris-HCl), the immunohistochemical reactions were visualised by using an Envision DAB kit (Dako, Tokyo, Japan). The sections were counterstained with haematoxylin. As a negative control for staining, the first antibodies were replaced with non-immune mouse immunoglobulin G (Dako). The sections were observed under a microscope (AxioImager A1; Carl Zeiss).

Lectin labelling of the retinal vasculature and adherent leucocytes

Leucocytes adhering to the retinal vasculature were imaged by perfusion labelling with fluorescein isothiocyanate-coupled concanavalin A lectin (Vector Laboratories, Burlingame, CA, USA).[27] After deep anaesthesia, the chest cavity was opened, a 20-gauge perfusion cannula was introduced into the aorta and a part of the liver was excised. After injection of 20 ml PBS to remove erythrocytes and non-adherent leucocytes, 20 ml of fluorescein isothiocyanate-conjugated concanavalin A lectin (40 μg ml^{-1}) was injected. Residual unbound concanavalin A was removed with PBS perfusion. After the eyeballs were enucleated, the retina was flat-mounted and imaged under a fluorescence microscope (Axiovert 40; Carl Zeiss).

Enzyme-linked immunosorbent assay

To detect serum antibodies to the rAAV2 capsid and the transgenic protein, ChR2, we coated enhanced protein-binding enzyme-linked immunosorbent assay plates with 10^9 viral particles per well of rAAV2 in 100 μl of 0.1 M sodium carbonate buffer (pH 9.6) and with 0.2 μg per well peptide coding for ChR2 by using a peptide coating kit (TaKaRa, Shiga, Japan) at 4 °C overnight. The wells were blocked with 10% fetal bovine serum-0.1% Tween in PBS for 30 min at 37 °C. Then, serum dilutions were added and incubated for 4 °C overnight. Dilutions of a rabbit anti-AAV2 capsid protein (American Research Product, Belmont, MA, USA) and a rabbit anti-ChR2 protein (TaKaRa) served as positive controls. The plates were incubated with horseradish peroxidase-conjugated anti-rabbit immunoglobulin G or anti-rat immunoglobulin G at 37 °C for 1 h in the presence of 3% goat serum. The reactions were visualised by adding one-step tetramethylbenzidine substrate (Promega, Tokyo, Japan). The reactions were stopped by adding 1 N HCl and read at 450 nm with a VERS Amax plate reader (Molecular Devices, Osaka, Japan). Each value was determined in triplicate.

Analysis of T lymphocytes

Peripheral blood $CD4^+$ cells have a central role in regulating the cell-mediated immune response to infection. Often known as helper T cells, they act on other cells of the immune system to promote various aspects of the immune response, including immunoglobulin isotype switching and affinity maturation and enhanced activity of natural killer cells and cytotoxic T cells. $CD4^+$ cells also act by releasing cytokines in response to antigenic stimulation. One of the major roles of $CD4^+$ cells is the activation of macrophages. During the course of hepatitis C virus infection, two different immunological statuses can be observed. In the acute phase of infection, $CD4^+$ helper T cells contribute to the induction and maintenance of a functional $CD8^+$ cell response. In the chronic phase, T regulatory ($CD4^+CD25^+$) cells suppress $CD8^+$ cell responses, and thereby help the virus to persist.[48] It is important to calculate these ratios to observe the immunological status.

Before and after the rAAV injection, peripheral blood was collected from the tail vein. Lymphocytes were isolated with PharmLyse (BD Bioscience, San Jose, CA, USA). After isolation, a mixture of monoclonal antibodies (mAbs) specific for CD3 (conjugated with Alexa Fluor 647; AbD Serotec, Oxford, UK), CD4 (conjugated with PE-Cy5; BD Bioscience), CD8a (conjugated with R-PE; BD Bioscience) and CD25 (conjugated with fluorescein isothiocyanate; BD Bioscience) was added to the cells, which were then incubated at 4 °C overnight. Flow-cytometric analysis was performed by using FACS Calibur (BD Bioscience) after washing the cells with PBS. For gating and calculation, CellQuest software (BD Bioscience) was used. In the FACS analysis, 10 000 cells were examined for each sample.

Statistical analysis

Statistical analysis was performed by using GraphPad Prism (GraphPad Software, San Diego, CA, USA). The criterion for statistical significance was $P<0.05$ by Dunnett multiple comparison test.

CONFLICT OF INTEREST

The authors declare no conflict of interest.

ACKNOWLEDGEMENTS

This work was partly supported by Grants-in-Aid for Scientific Research from the Ministry of Education, Culture, Sports, Science and Technology of Japan (nos. 21791664 and 21200022); Science and Culture and Special Coordination Funds for Promoting Science and Technology of the Japanese Government, Strategic Research Programme for Brain Sciences (SRPBS); the Ministry of Health, Labour and Welfare of Japan; and Japan Foundation for Aging and Health and the Programme for Promotion of Fundamental studies in Health Sciences of the National Institute of Biomedical Innovation (NIBIO). I also thank Teru Hiroi for technical support in animal treatment.

1 Hartong DT, Berson EL, Dryja TP. Retinitis pigmentosa. *Lancet* 2006; **368**: 1795–1809.
2 Santos A, Humayun MS, de Juan Jr E, Greenburg RJ, Marsh MJ, Klock IB *et al.* Preservation of the inner retina in retinitis pigmentosa. A morphometric analysis. *Arch Ophthalmol* 1997; **115**: 511–515.
3 Nagel G, Szellas T, Huhn W, Kateriya S, Adeishvili N, Berthold P *et al.* Channelrhodopsin-2, a directly light-gated cation-selective membrane channel. *Proc Natl Acad Sci USA* 2003; **100**: 13940–13945.

4 Bi A, Cui J, Ma YP, Olshevskaya E, Pu M, Dizhoor AM *et al.* Ectopic expression of a microbial-type rhodopsin restores visual responses in mice with photoreceptor degeneration. *Neuron* 2006; **50**: 23–33.
5 Tomita H, Sugano E, Yawo H, Ishizuka T, Isago H, Narikawa S *et al.* Restoration of visual response in aged dystrophic RCS rats using AAV-mediated channelopsin-2 gene transfer. *Invest Ophthalmol Vis Sci* 2007; **48**: 3821–3826.
6 Lagali PS, Balya D, Awatramani GB, Munch TA, Kim DS, Busskamp V *et al.* Light-activated channels targeted to ON bipolar cells restore visual function in retinal degeneration. *Nat Neurosci* 2008; **11**: 667–675.
7 Tomita H, Sugano E, Isago H, Hiroi T, Wang Z, Ohta E *et al.* Channelrhodopsin-2 gene transduced into retinal ganglion cells restores functional vision in genetically blind rats. *Exp Eye Res* 2010; **90**: 429–436.
8 Ishizuka T, Kakuda M, Araki R, Yawo H. Kinetic evaluation of photosensitivity in genetically engineered neurons expressing green algae light-gated channels. *Neurosci Res* 2006; **54**: 85–94.
9 Wang H, Peca J, Matsuzaki M, Matsuzaki K, Noguchi J, Qiu L *et al.* High-speed mapping of synaptic connectivity using photostimulation in Channelrhodopsin-2 transgenic mice. *Proc Natl Acad Sci USA* 2007; **104**: 8143–8148.
10 Tomita H, Sugano E, Fukazawa Y, Isago H, Sugiyama Y, Hiroi T *et al.* Visual properties of transgenic rats harboring the channelrhodopsin-2 gene regulated by the thy-1.2 promoter. *PLoS One* 2009; **4**: e7679.
11 Monville C, Torres E, Thomas E, Scarpini CG, Muhith J, Lewis J *et al.* HSV vector-delivery of GDNF in a rat model of PD: partial efficacy obscured by vector toxicity. *Brain Res* 2004; **1024**: 1–15.
12 Aiuti A, Bachoud-Lévi AC, Blesch A, Brenner MK, Cattaneo F, Chiocca EA *et al.* Progress and prospects: gene therapy clinical trials (part 2). *Gene Therapy* 2007; **14**: 1555–1563.
13 Alexander BL, Ali RR, Alton EW, Bainbridge JW, Braun S, Cheng SH *et al.* Progress and prospects: gene therapy clinical trials (part 1). *Gene Ther* 2007; **14**: 1439–1447.
14 Thomas CE, Ehrhardt A, Kay MA. Progress and problems with the use of viral vectors for gene therapy. *Nat Rev Genet* 2003; **4**: 346–358.
15 Koizumi K, Poulaki V, Doehmen S, Welsandt G, Radetzky S, Lappas A *et al.* Contribution of TNF-α to leukocyte adhesion, vascular leakage, and apoptotic cell death in endotoxin-induced uveitis *in vivo*. *Invest Ophthalmol Vis Sci* 2003; **44**: 2184–2191.
16 Zhang YC, Powers M, Wasserfall C, Brusko T, Song S, Flotte T *et al.* Immunity to adeno-associated virus serotype 2 delivered transgenes imparted by genetic predisposition to autoimmunity. *Gene Therapy* 2004; **11**: 233–240.
17 Damoiseaux JG, Cautain B, Bernard I, Mas M, van Breda Vriesman PJ, Druet P *et al.* A dominant role for the thymus and MHC genes in determining the peripheral CD4/CD8 T cell ratio in the rat. *J Immunol* 1999; **163**: 2983–2989.
18 Kim SA, Lim SS. T lymphocyte subpopulations and interleukin-2, interferon-γ, and interleukin-4 in rat pulpitis experimentally induced by specific bacteria. *J Endod* 2002; **28**: 202–205.
19 Toda A, Piccirillo CA. Development and function of naturally occurring CD4+CD25+ regulatory T cells. *J Leukoc Biol* 2006; **80**: 458–470.
20 Simpson E. A historical perspective on immunological privilege. *Immunol Rev* 2006; **213**: 12–22.
21 Caldwell RB, McLaughlin BJ. Permeability of retinal pigment epithelial cell junctions in the dystrophic rat retina. *Exp Eye Res* 1983; **36**: 415–427.
22 Caldwell RB, McLaughlin RJ, Boykins LG. Intramembrane changes in retinal pigment epithelial cell junctions of the dystrophic rat retina. *Invest Ophthalmol Vis Sci* 1982; **23**: 305–318.
23 Caldwell RB, Wade LA, McLaughlin BJ. A quantitative study of intramembrane changes during cell junctional breakdown in the dystrophic rat retinal pigment epithelium. *Exp Cell Res* 1984; **150**: 104–117.
24 Chang CW, Defoe DM, Caldwell RB. Retinal pigment epithelial cells from dystrophic rats form normal tight junctions *in vitro*. *Invest Ophthalmol Vis Sci* 1997; **38**: 188–195.
25 Nakai H, Yant SR, Storm TA, Fuess S, Meuse L, Kay MA. Extrachromosomal recombinant adeno-associated virus vector genomes are primarily responsible for stable liver transduction *in vivo*. *J Virol* 2001; **75**: 6969–6976.
26 Niemeyer GP, Herzog RW, Mount J, Arruda VR, Tillson DM, Hathcock J *et al.* Long-term correction of inhibitor-prone hemophilia B dogs treated with liver-directed AAV2-mediated factor IX gene therapy. *Blood* 2009; **113**: 797–806.
27 Satofuka S, Ichihara A, Nagai N, Yamashiro K, Koto T, Shinoda H *et al.* Suppression of ocular inflammation in endotoxin-induced uveitis by inhibiting nonproteolytic activation of prorenin. *Invest Ophthalmol Vis Sci* 2006; **47**: 2686–2692.
28 Reichelt W, Dettmer D, Bruckner G, Brust P, Eberhardt W, Reichenbach A. Potassium as a signal for both proliferation and differentiation of rabbit retinal (Muller) glia growing in cell culture. *Cell Signal* 1989; **1**: 187–194.
29 Hartig W, Grosche J, Distler C, Grimm D, el-Hifnawi E, Reichenbach A. Alterations of Muller (glial) cells in dystrophic retinae of RCS rats. *J Neurocytol* 1995; **24**: 507–517.
30 Hao LY, Hao XQ, Li SH, Li XH. Prenatal exposure to lipopolysaccharide results in cognitive deficits in age-increasing offspring rats. *Neuroscience* 2010; **166**: 763–770.
31 Beurel E, Jope RS. Lipopolysaccharide-induced interleukin-6 production is controlled by glycogen synthase kinase-3 and STAT3 in the brain. *J Neuroinflammation* 2009; **6**: 9.
32 Ni YQ, Gan DK, Xu HD, Xu GZ, Da CD. Neuroprotective effect of transcorneal electrical stimulation on light-induced photoreceptor degeneration. *Exp Neurol* 2009; **219**: 439–452.
33 Morimoto T, Miyoshi T, Sawai H, Fujikado T. Optimal parameters of transcorneal electrical stimulation (TES) to be neuroprotective of axotomized RGCs in adult rats. *Exp Eye Res* 2010; **90**: 285–291.
34 Wang J, Jiang S, Kwong JM, Sanchez RN, Sadun AA, Lam TT. Nuclear factor-kappaB p65 and upregulation of interleukin-6 in retinal ischemia/reperfusion injury in rats. *Brain Res* 2006; **1081**: 211–218.
35 Kaltschmidt C, Kaltschmidt B, Neumann H, Wekerle H, Baeuerle PA. Constitutive NF-kappa B activity in neurons. *Mol Cell Biol* 1994; **14**: 3981–3992.
36 O'Neill LA, Kaltschmidt C. NF-kappa B: a crucial transcription factor for glial and neuronal cell function. *Trends Neurosci* 1997; **20**: 252–258.
37 O'Garra A, Vieira P. Regulatory T cells and mechanisms of immune system control. *Nat Med* 2004; **10**: 801–805.
38 Sakaguchi S. Regulatory T cells: key controllers of immunologic self-tolerance. *Cell* 2000; **101**: 455–458.
39 Shevach EM. CD4+ CD25+ suppressor T cells: more questions than answers. *Nat Rev Immunol* 2002; **2**: 389–400.
40 Li W, Asokan A, Wu Z, Van Dyke T, DiPrimio N, Johnson JS *et al.* Engineering and selection of shuffled AAV genomes: a new strategy for producing targeted biological nanoparticles. *Mol Ther* 2008; **16**: 1252–1260.
41 Koga T, Koshiyama Y, Gotoh T, Yonemura N, Hirata A, Tanihara H *et al.* Coinduction of nitric oxide synthase and arginine metabolic enzymes in endotoxin-induced uveitis rats. *Exp Eye Res* 2002; **75**: 659–667.
42 Kügler S, Lingor P, Schöll U, Zolotukhin S, Bähr M. Differential transgene expression in brain cells *in vivo* and *in vitro* from AAV-2 vectors with small transcriptional control units. *Virology* 2003; **311**: 89–95.
43 Auricchio A, Hildinger M, O'Connor E, Gao GP, Wilson JM. Isolation of highly infectious and pure adeno-associated virus type 2 vectors with a single-step gravity-flow column. *Hum Gene Ther* 2001; **12**: 71–76.
44 Auricchio A, O'Connor E, Hildinger M, Wilson JM. A single-step affinity column for purification of serotype-5 based adeno-associated viral vectors. *Mol Ther* 2001; **4**: 372–374.
45 Sugano E, Tomita H, Ishiguro S, Abe T, Tamai M. Establishment of effective methods for transducing genes into iris pigment epithelial cells by using adeno-associated virus type 2. *Invest Ophthalmol Vis Sci* 2005; **46**: 3341–3348.
46 Papathanasiou ES, Peachey NS, Goto Y, Neafsey EJ, Castro AJ, Kartje GL. Visual cortical plasticity following unilateral sensorimotor cortical lesions in the neonatal rat. *Exp Neurol* 2006; **199**: 122–129.
47 Iwamura Y, Fujii Y, Kamei C. The effects of certain H(1)-antagonists on visual evoked potential in rats. *Brain Res Bull* 2003; **61**: 393–398.
48 Boettler T, Spangenberg HC, Neumann-Haefelin C, Panther E, Urbani S, Ferrari C *et al.* T cells with a CD4+CD25+ regulatory phenotype suppress *in vitro* proliferation of virus-specific CD8+ T cells during chronic hepatitis C virus infection. *J Virol* 2005; **79**: 7860–7867.

OPEN ACCESS Freely available online

PLoS one

Dissecting a Role for Melanopsin in Behavioural Light Aversion Reveals a Response Independent of Conventional Photoreception

Ma'ayan Semo[1]*, Carlos Gias[1], Ahmad Ahmado[1], Eriko Sugano[2], Annette E. Allen[3], Jean M. Lawrence[1], Hiroshi Tomita[2], Peter J. Coffey[1], Anthony A. Vugler[1]*

1 Department of Ocular Biology and Therapeutics, University College London-Institute of Ophthalmology, London, United Kingdom, **2** Institute for International Advanced Interdisciplinary Research, Tohoku University, Aoba-ku, Sendai, Japan, **3** Faculty of Life Sciences, University of Manchester, Manchester, United Kingdom

Abstract

Melanopsin photoreception plays a vital role in irradiance detection for non-image forming responses to light. However, little is known about the involvement of melanopsin in emotional processing of luminance. When confronted with a gradient in light, organisms exhibit spatial movements relative to this stimulus. In rodents, behavioural light aversion (BLA) is a well-documented but poorly understood phenomenon during which animals attribute salience to light and remove themselves from it. Here, using genetically modified mice and an open field behavioural paradigm, we investigate the role of melanopsin in BLA. While wildtype (WT), melanopsin knockout (*Opn4*$^{-/-}$) and *rd/rd cl* (melanopsin only (MO)) mice all exhibit BLA, our novel methodology reveals that isolated melanopsin photoreception produces a slow, potentiating response to light. In order to control for the involvement of pupillary constriction in BLA we eliminated this variable with topical atropine application. This manipulation enhanced BLA in WT and MO mice, but most remarkably, revealed light aversion in triple knockout (TKO) mice, lacking three elements deemed essential for conventional photoreception (*Opn4*$^{-/-}$ *Gnat1*$^{-/-}$ *Cnga3*$^{-/-}$). Using a number of complementary strategies, we determined this response to be generated at the level of the retina. Our findings have significant implications for the understanding of how melanopsin signalling may modulate aversive responses to light in mice and humans. In addition, we also reveal a clear potential for light perception in TKO mice.

Citation: Semo M, Gias C, Ahmado A, Sugano E, Allen AE, et al. (2010) Dissecting a Role for Melanopsin in Behavioural Light Aversion Reveals a Response Independent of Conventional Photoreception. PLoS ONE 5(11): e15009. doi:10.1371/journal.pone.0015009

Editor: Steven Barnes, Dalhousie University, Canada

Received August 18, 2010; **Accepted** October 11, 2010; **Published** November 29, 2010

Funding: This work was funded by the London Project to Cure Blindness (www.thelondonproject.org/) and the Lincy Foundation. The funders had no role in study design, data collection and analysis, decision to publish, or preparation of the manuscript.

Competing Interests: The authors have declared that no competing interests exist.

* E-mail: a.vugler@ucl.ac.uk (AAV); m.semo@ucl.ac.uk (MS)

Introduction

In the 1920's, Crozier and Pincus showed that neonatal rats with closed eyelids will move away from bright light along a gradient towards a less intensely illuminated target [1]. Adult rats retain an aversion to light [2,3], so strong that it can be used as a motivating factor in behavioural learning paradigms [4]. Like rats, adult mice also show behavioural light aversion (BLA) to acute (10–30 mins) light exposure in the open field [5,6]. Using mice, the "light/dark box test" has been employed extensively in drug development to identify putative anxiolytic compounds (see [5], reviewed in [7]) and more recently to investigate human photophobia in mouse models of migraine [8,9]. Despite the widespread application of this behavioural phenomenon, and its undoubted importance to the lives of nocturnal animals, little is known about the neural circuitry mediating BLA in rodents. Although one study to date has implicated both subcortical and cortical processing [10], the contribution of different photoreceptive components from the retina remains unclear.

In the mammalian retina, rods/cones of the outer retina are known to mediate image-forming vision [11,12], while photoreceptive melanopsin-expressing retinal ganglion cells (mRGCs) of the inner retina sub serve most non-image-forming responses to light [13,14,15,16,17]. If the eyes are enucleated bilaterally, then BLA in rats is abolished [10]. To date, only a few studies shed light on the important question of whether melanopsin alone could mediate this primitive non-image-forming response. These studies, from a variety of animal models, report mixed conclusions about a potential role for melanopsin in BLA.

A recent study investigating the role of melanopsin in non-image forming functions found that targeted destruction of melanopsin cells had no impact on the light:dark preference of mice [18]. This is in line with data from RCS rats showing a progressive loss of BLA over time, with no response detectable by 7 months [19]. Another study using *rd* mice also failed to report a significant light aversion response following exposure to illumination of 2800 Lux [20].

In contrast, spatial responses to light have been reported in *rd* mice given the choice between light and dark living/nesting areas over a 22 h period [21]. Here, retinal degenerate mice spent significantly more time in the dark than the illuminated area, a response that could be eliminated by enucleation. However, as *rd* mice retain a significant population of remodelled cones with identifiable presynaptic stuctures [22,23,24,25] they are unsatisfac-

tory for defining a role for melanopsin in BLA. In the present study we employ the *rd/rd cl* mouse, which lacks both rods and cones [15].

Melanopsin is a retinaldehyde-based, invertebrate-like photopigment [26,27] involved with mediating many responses to light that require a measure of general environmental irradiance [14,15, 28,29,30] and more recently, the ability of light to modulate sleep [31,32,33]. Importantly, an associative learning (Pavlovian conditioning) paradigm has shown that *rd/rd cl* mice can gradually learn to use a brief light stimulus to predict the onset of electric shocks [34]. Although melanopsin cells are thought to project mainly to subcortical, non-image forming centres of the brain, they may also signal luminance information to the visual cortex [35,36,37,38].

In humans, light aversion is often referred to as photophobia, a clinical term describing pain onset following light exposure in a number of conditions including migraine headache [39,40,41]. Recently, the melanopsin system has been implicated in the potentiation of migraine by light in blind patients [42] and although little is known about the neural circuitry of photophobia it is generally considered to require a convergence of information from optic and trigeminal nerves with associated cortical processing [40,42,43,44]. In addition, because sensory trigeminal afferents innervate muscles of the iris, sustained constriction caused by the pupillary light reflex (PLR) has also been implicated in causing the ocular discomfort felt following exposure to bright lights [40,41,45]. The term photophobia is also used to describe the sensation felt when we, as humans, enter an environment which is subjectively appraised as being "too bright", eliciting aversive behavioural responses such as looking away from bright light and squinting [46,47,48].

Our goal in the present study was to determine the extent to which melanopsin mediates BLA in mice. To achieve this, we developed a variation on an established protocol for measuring light aversion in mice [6], which now takes into account the behaviour of animals placed into complete darkness. We tested naïve wildtype (WT) mice, *rd/rd cl* mice (hereafter referred to as melanopsin only (MO)) [14,31], melanopsin knockout (MKO) mice (*Opn4*$^{-/-}$) [30] and as a control for the absence of light perception, triple knockout (TKO) mice, lacking melanopsin and functional rods/cones (*Opn4*$^{-/-}$ *Gnat1*$^{-/-}$ *Cnga3*$^{-/-}$). These mice have no significant PLR, circadian photoentrainment or masking responses [49]. In order to investigate if pupillary constriction is causally related to BLA, we also equalised this variable across genotypes by applying atropine bilaterally to the eyes.

Our experiments show that melanopsin alone can mediate a behavioural aversion to light that is associated with neural activation in the extended visual cortex. Analysis of temporal kinetics reveals that melanopsin acts slowly to increase light aversion over time, whereas rods/cones drive a more immediate aversive response. While MKO mice remain capable of BLA our analysis reveals that rods/cones and melanopsin are required for an aversive response characteristic of WT animals. Surprisingly, the addition of atropine increased BLA in WT, MO and TKO mice, with this new light perception in TKO's being associated with an enhancement of residual retinal activity. The retinal origin of light aversion behaviour in TKO mice was further investigated by either eliminating BLA with bilateral axotomy or generating a response comparable to that seen in wildtype animals by specifically activating retinal neurons using *Channelrhodopsin-2*.

Results

Melanopsin alone can drive the behavioural aversion to light

Animals were tested for BLA for 30 minutes in the open field apparatus shown in Figure 1A. This behaviour was assessed by comparing time spent in the dark back-half (BH) when the front-half (FH) was illuminated (light FH) with control conditions when the FH was maintained in darkness (dark FH).

Over the whole trial, WT normally-sighted animals spend the majority of their time (67%) in the dark BH of the arena when the FH is illuminated (Figure 1B). This is also significantly more time ($p<0.001$) than when the FH is maintained in darkness during which they spend only 34% of the time in the BH. The *rd/rd cl* animals, with only melanopsin as a functional photopigment (MO) do not spend the majority of their time in the dark when the FH is illuminated (46%), however a significant light-aversion response is revealed when this is compared to the amount of time that is spent in the BH when there is no illumination (27%) ($p<0.01$).

This result, together with previous observations of an impairment to BLA following lesions of visual cortex [10] prompted us to examine if melanopsin alone could drive activation of this structure in mice. This was achieved by examining light-induced c-Fos in the visual cortex of MO animals, a technique previously validated for normally sighted mice [50]. Here, using the same light source as that used for behavioural testing, we found a clear, melanopsin-driven c-Fos induction in medial visual/retrosplenial cortex (Figure S1).

Melanopsin is not required for the behavioural aversion to light

As seen in Figure 1, rods/cones also play a major role in BLA. When the behaviour of the congenic MO and WT mice are compared by two-way ANOVA there is a significant effect of genotype ($p<0.01$) and of light ($p<0.0001$), with Bonferroni's multiple comparison tests confirming a significant reduction in time spent in the dark BH when the FH is illuminated in the MO (46%) compared to the WT (67%) mice ($p<0.01$). In control conditions, when the entire arena is in darkness there is no significant difference in behaviour between MO and WT mice, both seeming to retain a preference for the FH.

Animals lacking melanopsin (MKO) spend significantly more time (60%, $p<0.05$) in the dark BH when light is on in the FH (Figure 1B), than when there is no illumination (only 28% of time spent in BH). This finding shows that although melanopsin alone can mediate BLA, the presence of this photopigment is not a requirement for this response to occur. As anticipated, in TKO mice (lacking melanopsin and normal rod/cone function), there is no response to illumination in the FH, with these mice spending similar amounts of time ($p>0.05$) in the BH whether the FH is in darkness or light (29 versus 21% of the time).

Interestingly, regardless of whether the light was on or off, TKO mice spend most of their time in the open FH of the arena, as do the other genotypes in the complete darkness control condition. This phenomenon holds true regardless of which side of the arena animals are first placed (data not shown). To the best of our knowledge, this consistent behaviour has not been reported previously and should be taken into account when interpreting data derived from light:dark choice tests of a similar design to ours.

Temporal kinetics of light aversion in mice

To investigate the behaviour of mice during the course of the 30-minute trial, data were binned into 6, 5-minute bins throughout the trial (Figure 2A–D). Results of the associated regression analysis are summarised in table 1. Under control conditions (complete darkness), in all genotypes, animals failed to change the amount of time spent in the BH (slopes of regression lines are not significantly non-zero). However, when there is light in the FH of the arena, both WT and MO mice show a positive correlation with duration of the trial, spending more time in the

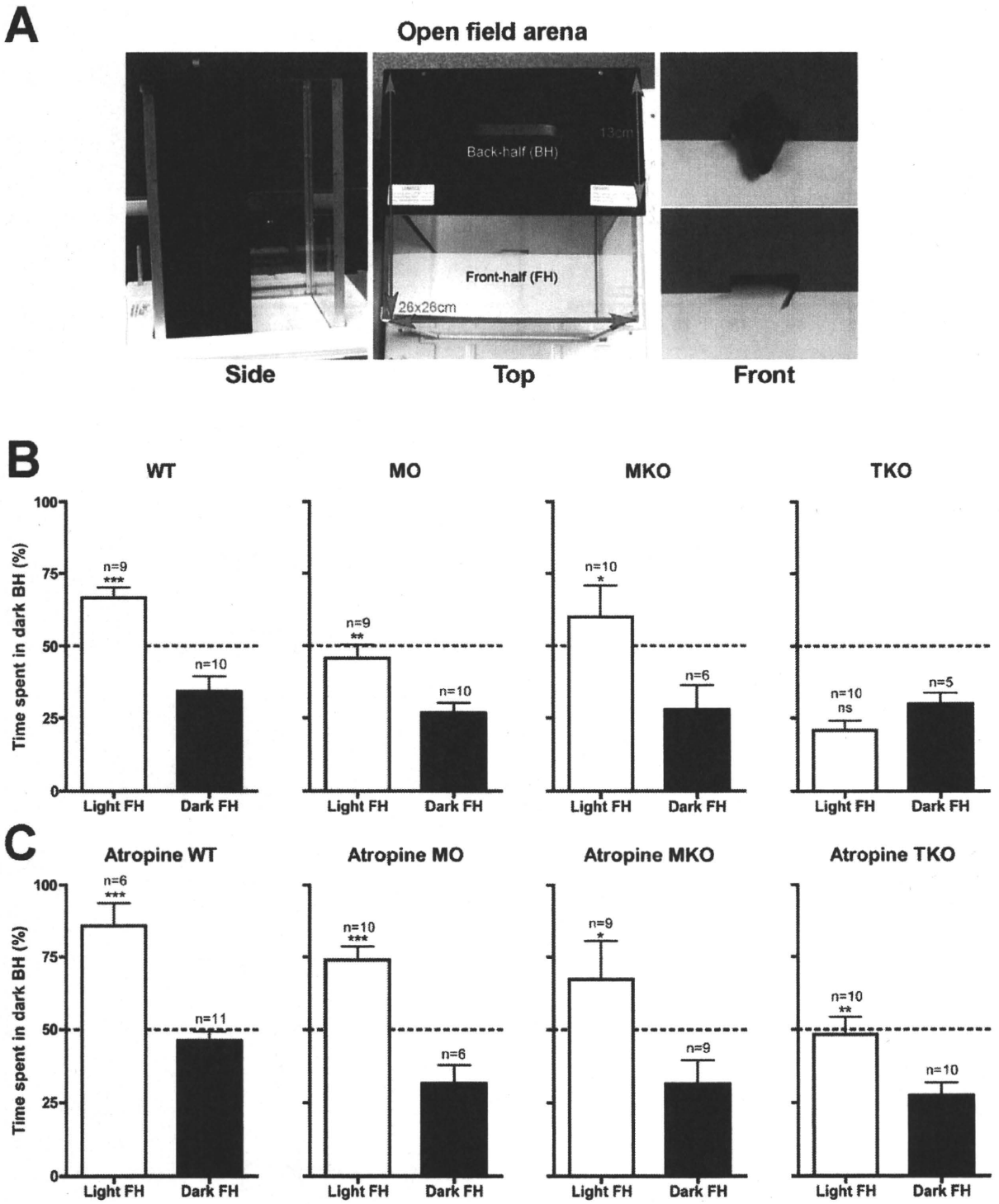

Figure 1. Role of melanopsin in the behavioural aversion to light in mice. (**A**) Open field apparatus: animals were placed into the front-half (FH) of the arena and remained there for 30 minutes. Time spent in the back-half (BH) of the arena was recorded. (B) and (C) Average (±SEM) percentage of time spent in the dark BH of the arena during the 30-minute trial. The FH is either illuminated, white bars (light FH), or in darkness, black bars (dark FH). (**B**) In untreated animals photophobic behaviour is evident in wildtype (WT), melanopsin only (MO) *rd/rd cl* mice, and melanopsin knockout (MKO) mice. Triple knockout (TKO) mice, lacking melanopsin and functional rods and cones show no aversion to light. (**C**) Atropine significantly increases aversive behaviour in WT, MO, and TKO mice. In MKO mice, atropine increases the average aversive behaviour but this does not reach significance. Atropine does not significantly affect behaviour when the FH is in darkness in any of the genotypes. Stars (*) indicate significance levels (Student's *t*-test): * $p<0.05$; ** $p<0.01$; *** $p<0.001$.
doi:10.1371/journal.pone.0015009.g001

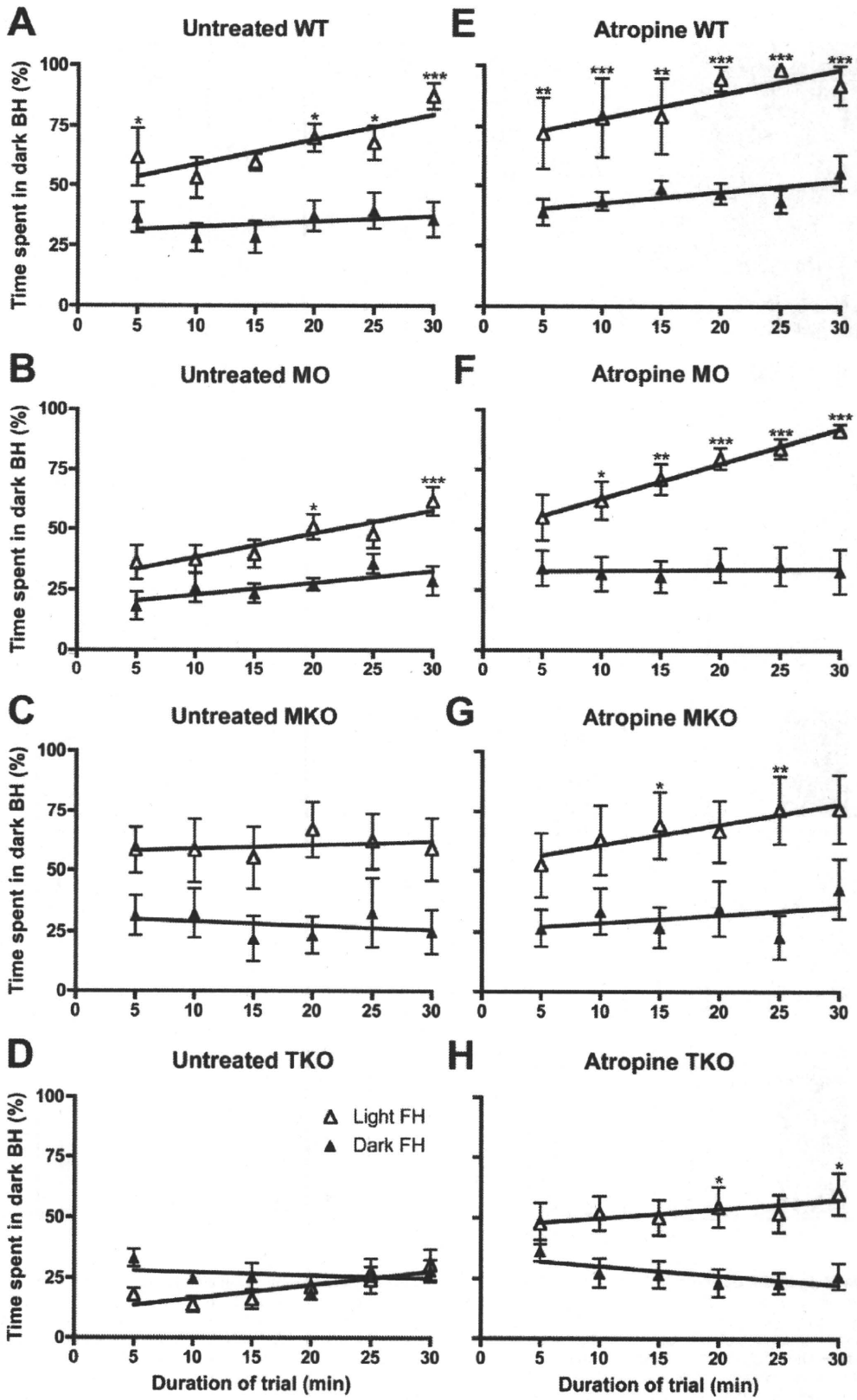
A
Untreated WT
E
Atropine WT
B
Untreated MO
F
Atropine MO
C
Untreated MKO
G
Atropine MKO
D
Untreated TKO
H
Atropine TKO
Light FH
Dark FH
Time spent in dark BH (%)
Duration of trial (min)